



January 2019

Reservoir Characterization And Simulation Of Enhanced Oil Recovery For Bakken

Runxuan Sun

Follow this and additional works at: <https://commons.und.edu/theses>

Recommended Citation

Sun, Runxuan, "Reservoir Characterization And Simulation Of Enhanced Oil Recovery For Bakken" (2019). *Theses and Dissertations*. 2488.

<https://commons.und.edu/theses/2488>

This Thesis is brought to you for free and open access by the Theses, Dissertations, and Senior Projects at UND Scholarly Commons. It has been accepted for inclusion in Theses and Dissertations by an authorized administrator of UND Scholarly Commons. For more information, please contact zeinebyousif@library.und.edu.

**RESERVOIR CHARACTERIZATION AND SIMULATION OF ENHANCED OIL
RECOVERY FOR BAKKEN**

by

Runxuan Sun

Bachelor of Science, China University of Petroleum (Beijing), 2017

A Thesis

Submitted to the Graduate Faculty

of the

University of North Dakota

In partial fulfillment of the requirements

for the degree of

Master of Science

In Petroleum Engineering

Grand Forks, North Dakota

May

2019

Copyright 2019 Runxuan Sun

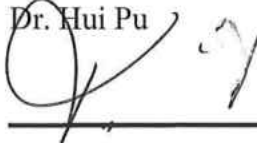
or

c 2019 Runxuan Sun

This thesis, submitted by Runxuan Sun in partial fulfillment of the requirements for the Degree of Master of Science in Petroleum Engineering from the University of North Dakota, has been read by the Faculty Advisory Committee under whom the work has been done and is hereby approved.



Dr. Hui Pu



Dr. Rasouli Vamegh



Dr. Kegang Ling

This thesis is being submitted by the appointed advisory committee as having met all of the requirements of the School of Graduate Students at the University of North Dakota and it hereby approved.



Dean of the School of Graduate Studies

4/24/19

Date

PERMISSION

Title Reservoir Characterization and Simulation of Enhanced Oil Recovery for Bakken

Department Petroleum Engineering

Degree Master of Science

In presenting this thesis in partial fulfillment of the requirements for a graduate degree from the University of North Dakota, I agree that the library of this University shall make it freely available for inspection. I further agree that permission for extensive copying for scholarly purposes may be granted by the professor who supervised my thesis work or, in his absence, by the Chairperson of the department or the dean of the School of Graduate Studies. It is understood that any copying or publication or other use of this thesis or part thereof for financial gain shall not be allowed without my written permission. It is also understood that due recognition shall be given to me and to the University of North Dakota in any scholarly use which may be made of any material in my thesis.

Runxuan Sun

04/23/2019

TABLE OF CONTENTS

LIST OF FIGURES.....	vii
LIST OF TABLES.....	xi
ACKNOWLEDGEMENTS.....	xii
ABSTRACT.....	xiii
CHAPTER	
I. INTRODUCTION	1
1.1 Statement of the Problem.....	1
1.2 Objectives.....	2
1.3 Organization of the Thesis	2
II. LITERATURE REVIEW.....	4
2.1 Geologic Background of the Bakken Formation.....	4
2.2 Past Simulation of CO ₂ Huff-n-Puff.....	8
2.3 Past Simulation of Surfactant Flooding.....	10
2.4 Review of Embedded Discrete Fracture Model (EDFM).....	11
III. CHARACTERIZATION OF BAKKEN SAMPLES.....	13
3.1 Scanning Electron Microscope (SEM).....	13
3.2 Computed Tomography (CT) Scans.....	17
3.3 Thin Section Petrography.....	20
IV. RESERVOIR SIMULATION OF FIELD SCALE CO ₂ HUFF-N-PUFF PROCESS.....	27

4.1 Description of the Simulation Model	27
4.2 Fluid Model Setup.....	29
4.3 EDFM Validation.....	30
4.4 History Match.....	33
4.5 Sensitivity Analysis.....	39
V. RESERVOIR SIMULATION OF FIELD SCALE SURFACTANT HUFF- N-PUFF PROCESS	53
5.1 Description of the Simulation Model.....	53
5.2 Laboratory Data.....	54
5.3 EDFM Validation.....	56
5.4 History Match.....	58
5.5 Wettability Alteration.....	61
5.6 Surfactant Effectiveness Verification.....	64
5.7 Sensitivity Analysis.....	66
VI. CONCLUSIONS AND RECOMMENDATIONS.....	76
REFERENCES.....	81

LIST OF FIGURES

Figure	Page
1. The boundaries of Bakken Formation in the Williston Basin. The shaded red portion indicates the active Bakken play, and the structure contour lines show the Williston Basin (Cosima et al., 2013).....	4
2. Generalized stratigraphic column for the Bakken petroleum system. FB = False Bakken, S = Scallion, UBS = Upper Bakken shale, MB-A through MB-F = Middle Bakken, LBS = Lower Bakken shale, PH = Pronghorn, UTF = Upper Three Forks, MTF = Middle Three Forks (Stephen et al., 2011).....	6
3. West to the east diagrammatic cross section of the Bakken petroleum system. The maturity line (red line) across the basin depending on the geothermal information. The dashed line represents the overpressured interval (Stephen et al., 2011).....	7
4. Bakken rock sample SEM results of well 1.....	14
5. SEM results of Bakken rock sample from well 2.....	15
6. Bakken rock sample SEM results of well 3.....	16
7. Steps of a 3D model reconstruction for the middle Bakken rock sample through CT scans method (from a to d).....	18
8. Different rock properties distribution characterization of the Middle Bakken rock sample through CT scans.....	19
9. Quantization of the pore distribution and pore throat distribution.....	19
10. Metallurgical microscope results of thin section observation under different light sources (well 1).....	22
11. Metallurgical microscope results of thin section observation under different light sources (well 2).....	23
12. Metallurgical microscope results of thin section observation under different light sources (well 3).....	25
13. Relative permeability curves used in this study (Yu et al., 2014).....	29
14. Comparison of fracture modelling between EDFM and LGR.....	31
15. Comparison of well performance and BHP between LGR and EDFM.....	33

16. A field-scale reservoir model with one horizontal well penetrated 30 bi-wing hydraulic fractures.....	34
17. Oil flow rate comparison between the actual well data and simulation results.....	34
18. Comparison of gas flow rate and bottomhole pressure between real well production data and simulation model results.....	35
19. Pressure distribution at the end of the history match.....	35
20. A section model with a horizontal well and 2 bi-wing hydraulic fractures.....	36
21. Oil flow rate comparison between actual well data and section model results.....	37
22. Comparison of gas flow rate and bottomhole pressure between modified well production data and simulation model results.....	38
23. Section Model pressure distribution at the end of the history match.....	38
24. Effect of different CO ₂ injection rates on CO ₂ Huff-n-Puff effectiveness.....	40
25. Effect of different CO ₂ injection rate on wellbore and reservoir pressure.....	41
26. Effect of different CO ₂ injection time on CO ₂ Huff-n-Puff effectiveness.....	43
27. Effect of different CO ₂ injection time on wellbore and reservoir pressure.....	43
28. Effect of different CO ₂ injection time on reservoir CO ₂ saturation.....	44
29. Effect of different CO ₂ soaking time on CO ₂ Huff-n-Puff effectiveness.....	45
30. Effect of different CO ₂ soaking time on wellbore and reservoir pressure.....	46
31. Effect of different numbers of CO ₂ Huff-n-Puff cycles on CO ₂ Huff-n-Puff effectiveness.....	47
32. Effect of different CO ₂ molecular diffusions on CO ₂ Huff-n-Puff effectiveness.....	49
33. Effect of different CO ₂ molecular diffusions on the cumulative CO ₂ backflow.....	50
34. Comparison of CO ₂ gas mole fraction distribution after 7000 days CO ₂ Huff-n-Puff.....	51
35. Rank of impacts of five uncertain parameters on incremental oil recovery factor.....	52
36. Comparison of well performance and BHP between LGR and EDFM.....	55

37. A field-scale reservoir model with a horizontal well and 30 bi-wing hydraulic fractures.....	56
38. Oil flow rate comparison between actual Middle Bakken well data and model results.....	57
39. Comparison of gas flow rate and bottomhole pressure between real well production data and simulation model results.....	57
40. A section model with a horizontal well and two bi-wing hydraulic fractures.....	58
41. Cumulative oil production comparison between different grid layers with surfactant flooding case.....	59
42. Oil flow rate comparison between actual well data and section model results.....	60
43. Comparison of gas flow rate and bottomhole pressure between modified well production data and simulation model results.....	61
44. Three inputted oil-water relative permeability curves for different rock wettability conditions.....	63
45. Three inputted capillary pressure curves for different rock wettability conditions (Masalmeh., 2002; Anderson., 2006).....	63
46. The Langmuir adsorption isotherm curve.....	64
47. Oil recovery factor comparison between the primary production and surfactant flooding case.....	65
48. Adsorbed mole of surfactant and IFT in the end of surfactant flooding.....	66
49. The comparison of three different Langmuir adsorption isotherm curves.....	67
50. Effect of different surfactant adsorption on surfactant Huff-n-Puff effectiveness.....	68
51. Effect of different CO2 injection times on CO2 Huff-n-Puff effectiveness.....	70
52. Effect of different CO2 soaking times on CO2 Huff-n-Puff effectiveness.....	71
53. Effect of different numbers of CO2 Huff-n-Puff cycles on CO2 Huff-n-Puff effectiveness.....	72
54. Effect of different surfactant injection rate on CO2 Huff-n-Puff effectiveness.....	73
55. Effect of surfactant concentration on surfactant Huff-n-Puff effectiveness.....	74

56. Rank of impacts of six uncertain parameters on incremental oil recovery factor.....75

LIST OF TABLES

Table	Page
1. Middle Bakken rock sample analysis by Avizo digital rock processing.....	20
2. Field case reservoir model parameters.....	28
3. Compositional data for the Middle Bakken formation.....	30
4. Binary interaction parameters for Middle Bakken oil.....	30
5. Section history matching parameters.....	37
6. Field case reservoir model parameters.....	53
7. Section model parameters.....	60
8. Surfactant IFT table.....	63
9. Time steps comparison between surfactant flooding and primary production.....	65
10. Parameters and their range for surfactant Huff-n-Puff sensitivity analysis.....	67

ACKNOWLEDGMENTS

I wish to express my sincere appreciation to the members of my Advisory Committee for their guidance and support during my time in the master's program at the University of North Dakota.

To my mom Xiaohong Zhu and my dad Dongsheng Sun,
The world's best parents!

ABSTRACT

The Bakken formation is one of the largest unconventional resources in the world with approximately 92 billion barrels of recoverable oil. However, the primary oil recovery factor remains as low as less than 10% of the original oil in place (OOIP). Given the vast Bakken resources and low primary oil recovery, there is a need and enormous potential for the enhanced oil recovery (EOR) in Bakken.

Two comprehensive numerical compositional models were built for the simulation CO₂ Huff-n-Puff and cyclic surfactant injection in an actual Middle Bakken horizontal well. A good history match of primary production was obtained. Embedded Discrete Fracture Model (EDFM) method was used to efficiently handle hydraulic fractures using non-neighboring connections as a new technique in this simulation study.

The EDFM method is faster than the traditional local grid refinement method. The results of CO₂ Huff-n-Puff and cyclic surfactant injection processes are compared and discussed. The simulation results show that both enhanced oil recovery processes can significantly increase oil recovery.

CHAPTER I

INTRODUCTION

1.1 Statement of the Problem

The oil production rate declined sharply in a very short of time after the well starts producing, resulting in low oil recovery factor in the Bakken Formation. Bakken Formation is one of the largest tight oil reservoirs in the U.S, which is typically characterized by low porosity (<10%) and low permeability (<0.1 mD) (David et al., 2013). The Bakken is among the most significant oil discoveries in the United States in the past 40 years and has made North Dakota the second-highest oil-producing state in the U.S. (DuBose, 2012). In 2008, the technically recoverable oil reported can reach 3.65 billion barrels (Pollastro et al., 2008). This number increased to 11.43 billion barrels in 2013 (Gaswirth et al., 2013), and 92 billion barrels in 2015 (Government of Saskatchewan Report, 2015). The advanced technique of horizontal well development and multi-stage hydraulic fracturing helps to increase the number of recoverable oil tremendously during this period. Moreover, the average daily oil production growth from 175 bbl/day in 1953 to 1106836 bbl/day in 2018 (DMR, 2018). However, significant amount of oil is still remaining in the reservoir due to low oil recovery. Due to such drastic decline of oil production rate, the ultimate recovery factor is around 7% (Sorensen et al., 2014), which is far lower than the oil recovery rate of the conventional reservoirs (Jacobs, 2016). Given this massive amount of oil remaining in place, it is important to develop some new advanced techniques to enhance the oil recovery factor.

1.2 Objectives

In this research, the primary objective was to counter the problem of low oil recovery factor, several EOR methods were studied, including chemical flooding and CO₂ flooding. The software used were CMG-GEM, CMG-STARS, CMG-Winprop, EDFM and Paraview. The CMG-Winprop was used to generate the fluid model, and the EDFM can build up the fracture model. These two models can be imported to CMG in a nonintrusive way. The reservoir model and other properties were built in CMG-GEM and CMG-STARS. Different factors were tested in the sensitivity study section by varying the factors within their range. Sufficient case studies were conducted in this thesis, to figure out the premium EOR for a limited time.

1.3 Organization of the thesis

A total of six chapters constitutes this thesis. After Chapter 1 of the introduction, a literature review of different vital methods used in this research is presented in Chapter 2, which concludes the past EOR simulation works. In Chapter 3, the characterization of the Bakken core samples is analyzed based on a series of different experiment measurements. In Chapter 4, a CO₂ Huff-n-Puff study is presented that focuses on history matching and sensitivity test. The EDFM method can help to create the most direct and effective fracture model. It helps the simulating process in CMG-GEM to run more smoothly and successfully. In Chapter 5, a surfactant flooding study is conducted, considering the modification of the rock wettability and interfacial tension. A history match and sensitivity test are also studied in this study, in order to optimize the surfactant EOR. Finally, Chapter

6 summarizes the conclusions in this research and gives some constructive recommendations for future study.

CHAPTER II

LITERATURE REVIEW

2.1 Geologic Background of the Bakken Formation

The Bakken Formation located in the Williston Basin, which the chronostratigraphic unit is from the Late Devonian to the Early Mississippian. The Williston Basin extends over parts of North Dakota, Montana, and the Canadian Provinces of Saskatchewan and Manitoba (Cosima et al., 2013). As shown in **Fig. 1**, the current boundaries of the active Bakken play is shaded in red, and the Williston Basin is contoured by green lines in a large, oval shape.

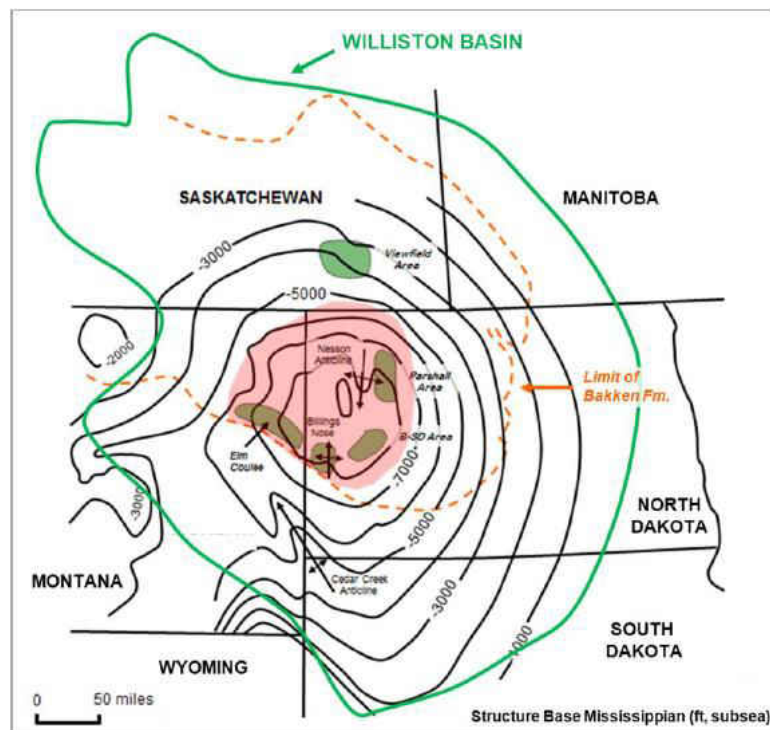


Fig. 1 The boundaries of Bakken Formation in the Williston Basin. The shaded red portion indicates the active Bakken play, and the structure contour lines show the Williston Basin (Cosima et al., 2013).

The Williston Basin is an intracratonic sag basin and precipitated a sediment thickness of over 16,000 ft. There is an almost complete stratigraphic record from Cambrian to Tertiary time (Carlson et al., 1965; LeFever et al., 1965).

The Bakken oil reservoir comprised of three formations, which are the Three Forks, Bakken, and lower Lodgepole formation from bottom to top, as shown in **Fig. 2**. The Bakken formation can be divided into three layers: the Lower Bakken shale, the Middle Bakken and the Upper Bakken shale. The Sanish sand which known as ‘Lower Bakken silt’ can also seem like part of the Bakken formation in some paper.

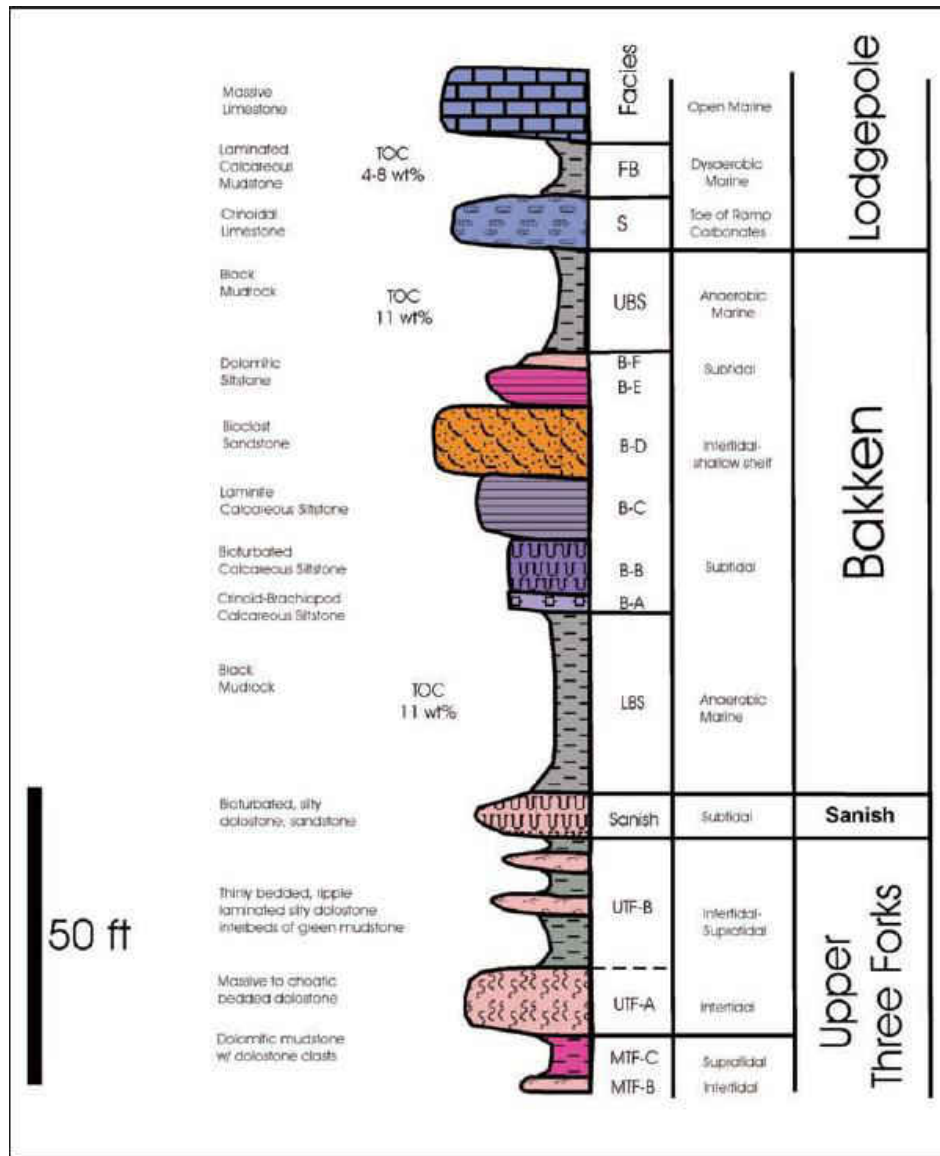


Fig. 2 Generalized stratigraphic column for the Bakken petroleum system. FB = False Bakken, S = Scallion, UBS = Upper Bakken shale, MB-A through MB-F = Middle Bakken, LBS = Lower Bakken shale, PH = Pronghorn, UTF = Upper Three Forks, MTF = Middle Three Forks (Stephen et al., 2011).

The Upper Bakken and Lower Bakken are two black shale layers and also source rocks of the Bakken oil reservoir. The total organic carbon (TOC) content can reach 11 to 12 weight per cent (Schmoker et al., 1983). The Middle Bakken layer is the main oil reservoir in the Bakken Formation. It is a very thin, widespread unit as shown in **Fig. 3**. The maximum thickness can only reach 150 ft (Pitman et al., 2001). The source rock maturity line is from

west to east across the basin, depending on the geothermal gradients. The Middle Bakken layer was deposited in a shallow-water setting following a rapid sea-level drop, leading to a regressive event (Meissner et al., 1984; Smith et al., 1996). The mineralogy of the Middle Bakken is variable (LeFever., 2007), so the rock type in this unit can be silty dolomite to calcareous sandstones in place. The Bakken formation is typically characterized by low porosity (<10%) and low permeability (<0.1 mD) in North America (David et al., 2013). However, the Hydraulic-fracture stimulation and horizontal drilling significantly improve the low porosity and permeability reservoir of the Bakken oil reservoir to be a ‘sweet spots’ (Murray., 1968; Meissner., 1978; Cramer., 1986, 1991).

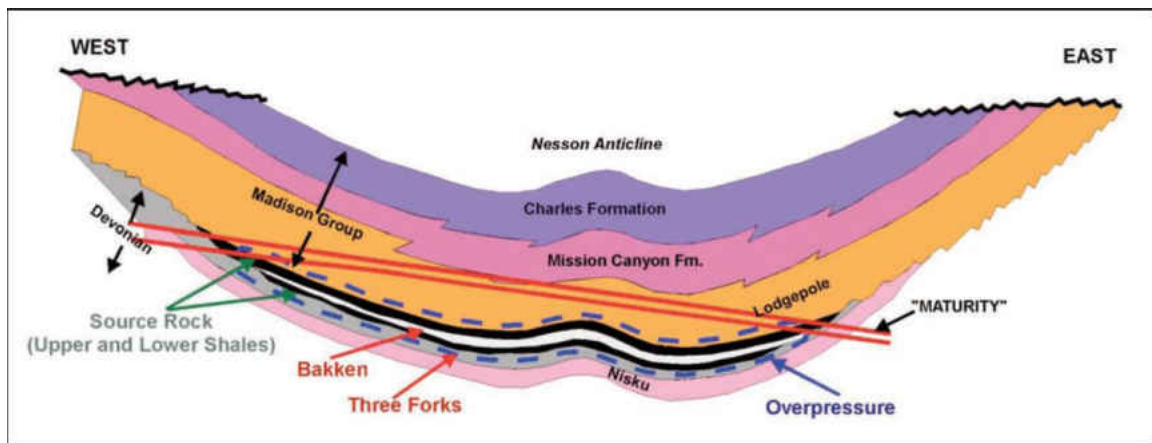


Fig. 3 West to the east diagrammatic cross section of the Bakken petroleum system. The maturity line (red line) across the basin depending on the geothermal information. The dashed line represents the overpressured interval (Stephen et al., 2011).

People thought Bakken shales sourced reservoirs in the Bakken and entire Madison Group (Dow., 1974; Williams., 1974; Meissner., 1978). However, Price (1994, 1999) presented evidence and claimed that most of the oil generated in the Bakken Formation had not immigrated far in the vertical direction. Therefore, it is a big potential to recover oil from the Bakken Formation.

2.2 Past Simulation of CO₂ Huff-n-Puff

Wide interest in the application of Enhanced Oil Recovery (EOR) techniques like CO₂ injection EOR has aroused due to a large amount of oil remaining in place (Alfarge et al, 2017a). In this case, lots of researchers have paid their efforts for evaluating the CO₂ Huff-n-Puff EOR method, and trying to maximize the oil recovery factor (Yu et al., 2014).

CO₂ Huff-n-Puff or cyclic injection process is an advanced and effective way comparing with the current continuous CO₂ flooding. There are three steps to operate the CO₂ huff-n-puff process: CO₂ injection, CO₂ soaking, and Production. The cyclic CO₂ injection was designed by Monger et al. (1988) to increase the oil recovery in tight oil reservoir as early as 1988, and they claimed that it is a feasible and beneficial method. The natural gas Huff-n-Puff injection in waterflooded cores was conducted using two injection cycles and found that approximately 40% of waterflood residual oil can be recovered (Haines et al., 1990). The approach of CO₂ EOR in tight oil reservoir has received much attention because of the low viscosity and large injectivity of CO₂ (Kurtoglu et al., 2013; Song and Yang, 2013; Adekunle and Hoffman, 2014).

Moreover, a pilot field test has already been conducted in a low permeability offshore field using CO₂ Huff-n-Puff process which has shown favorable results (Le et al., 2013). Although CO₂ EOR has been well investigated in conventional oil reservoirs, it is still a new challenging topic in unconventional oil reservoirs (Yu et al., 2018). All logic and reasonable steps of research, such as experimental investigations, simulation studies, and pilot tests for discovering the feasibility and practicability of different EOR methods have just started over the last decade (Alfarge et al., 2017b).

Besides, much more efforts have been devoted for simulation studies of CO₂ and gas injection EOR in the unconventional reservoirs in order to examine the recovery mechanisms and feasibility (Shoaib and Hoffman, 2009; Wang et al., 2010; Ren et al., 2011; Chen et al., 2014). The effects of heterogeneous reservoir properties on CO₂ Huff-n-Puff performance was investigated by Chen et al. (2014) used a compositional reservoir simulator. Wan et al. (2015) found that matrix/fracture and matrix/matrix diffusion play an essential role in the oil recovery process through gas injection in the fractured shale oil reservoirs using the dual-permeability simulator. Yu (2014, 2015) built a numerical reservoir model with multiple hydraulic fractures for Bakken Formation to simulate CO₂ Huff-n-Puff process and found out that the CO₂ molecular diffusion effect is an essential factor to improve the oil recovery in the tight oil reservoir. The continuous injection is not the best approach to improve the oil recovery due to the long propagation time caused by the tight oil reservoir with low porosity and permeability (Sanchez., 2014). The continuous CO₂ flooding is only favorable for oil recovery in the reservoir with permeability higher than 0.1 mD, which in turn that CO₂ huff-n-puff can have a high performance with permeability lower than 0.01 mD (Zuloaga et al., 2016, 2017). Zhang (2017) found that the capillary pressure causes the increase of oil recovery performance in CO₂ huff-n-puff, according to the investigation of nanopore confinement effect.

However, there is a large gap of EOR between lab-scale and field-scale that needs to be addressed (Atsushi et al., 2018). Alharthy et al. (2017) conducted a comprehensive study of CO₂ EOR from the laboratory to field scales. The CO₂ solvent-soaking-experiments using the Bakken cores showed that molecular diffusion significantly contributes to the

recovery, but the history-matched field scale model showed little effects of molecular diffusion on the incremental oil recovery.

2.3 Past Simulation of Surfactant Flooding

Surfactant flooding can reduce the IFT between the aqueous and oil phases in Chemical Enhanced Oil Recovery (CEOR) (Ngo et al., 2017). The wettability of the rock can also be influenced by the surfactant to help in changing the fluid properties, reducing the advanced drag, reducing the IFT and lowering the mobility of capillary trapped oil (Cheraghian et al., 2014). Also, it can reduce oil-water interfacial tension without changing the wettability state, like the capillary desaturation effect, as the surfactant solution is at the critical micelle concentration (CMC) (Mohammad et al., 2017). Moreover, some surfactant solutions may alter wettability state without a significant changing in fluid pair IFT (Singh et al., 2016). Yuan and Lee reviewed the contact angle measurement (basic and advanced) techniques for wettability determination of the materials at macro, micro and nanoscale. The contact angle is the primary measurement of the wettability. The surfactant which can change the wettability effectively also needs to withstand the high temperature and high salinity environment at the same time (Sharma et al., 2013). The surfactants affects the interaction between the fluid and solid phases by placing themselves at the interface, the continuity between the nanoparticles and the base fluid can also be increased (Jung et al., 2018). Moreover, numerical efforts have been devoted to simulation studies of surfactant and nanoparticle injection CEOR in unconventional reservoirs in order to examine recovery mechanisms and feasibility (Datta-Gupta et al., 1986; Mojdeh et al., 1996). A 3-D multifunctional compositional numerical simulator of alkali/surfactant/polymer flooding

was established, and various mechanisms and parameter effects were tested (Yuan et al., 1995). Abdulkareem (2012) used the University of Texas Chemical Flooding Simulator: UTCHEM (PGE, 2007) simulated surfactant and polymer flooding to find an optimized surfactant concentration. Wang et al. (2015) also used the UTCHEM simulator to investigate the surfactant and polymer injection based on a reservoir condition. Adibhatla et al. (2005) developed a 3-D numerical simulator to model the surfactant flooding EOR by lowering the oil-water IFT and by altering the wettability of the matrix block to water-wet. A three-phase hysteresis model was built to predict the cycle-dependent relative permeability curves, and the dynamic Land coefficient was set to each cycle to modify the phase saturation (Land, 1971). Beygi et al. (2015) discussed a complete list of two- and three-phase hysteresis models.

2.4 Review of Embedded Discrete Fracture Model (EDFM)

Compositional simulation has been widely used to deal with many EOR problems, such as gas flooding and chemical flooding. However, the substantial computational burden makes it challenging to conduct the field case model with multiple hydraulic fractures and comprehensive well controls (Yu et al., 2014). Some important underlying physics might be masked due to the over-simplification of the simulation models (Atsushi et al., 2018), like complex fracture geometries which are often created during the hydraulic fracturing process (Cipolla and Wallace, 2014; Wu and Olson, 2016) and various hydraulic fracture height in different layers (Yue et al., 2018). In order to overcome these issues, a state-of-the-art embedded discrete fracture model (EDFM) was developed (Moinfar et al., 2014; Cavalcante Filho et al., 2015; Shakiba and Sepehrnoori, 2015; Yu et al., 2017). The EDFM

method can model complex fractures conveniently (Xu, 2015; Zuloaga-Molero et al., 2016; Zhang et al., 2017c; Xu et al., 2017a, 2017b).

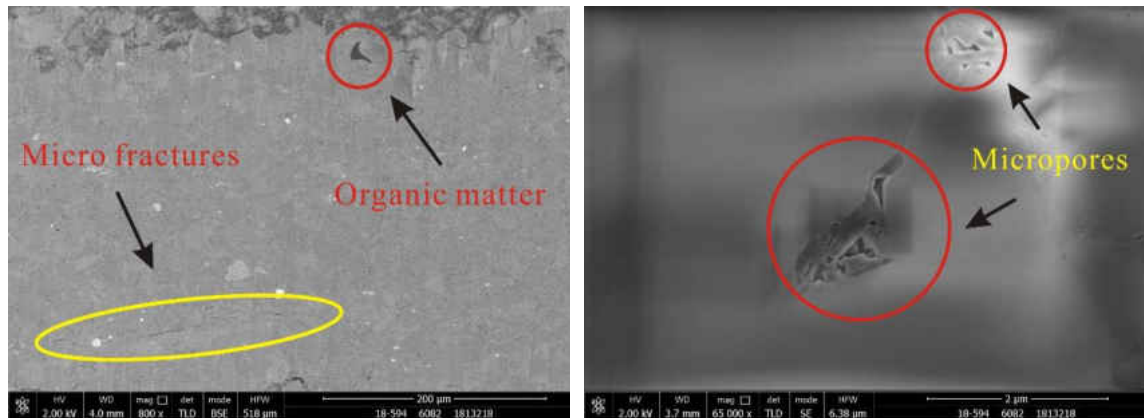
The central principle of the EDFM method is using the finite-element or finite-difference method to create discrete-fracture models (DFMs) to describe complex fractures in the reservoir (Xu et al., 2017). Unstructured grids can appropriately model the fractures (Matthai et al., 2005; Sandve et al., 2012). The EDFM can not only honor the accuracy of DFMs, but also keeping the efficiency of structured gridding (Lee et al., 2001; Hajibeygi et al., 2011). The EDFM can be used for 3D simulations including slanted fractures, and can also simulated the compositional reservoir model (Moinfar et al., 2014). Panfili et al. (2014) applied the EDFM to a commercial simulator, and also used it with corner-point geometry grids. Jiang et al. (2014) developed the EDFM with dual-continuum and multiple interacting continua (MINC) to model the complex fractures in shale reservoirs.

CHAPTER III CHARACTERIZATION OF BAKKEN SAMPLES

3.1 Scanning Electron Microscope (SEM)

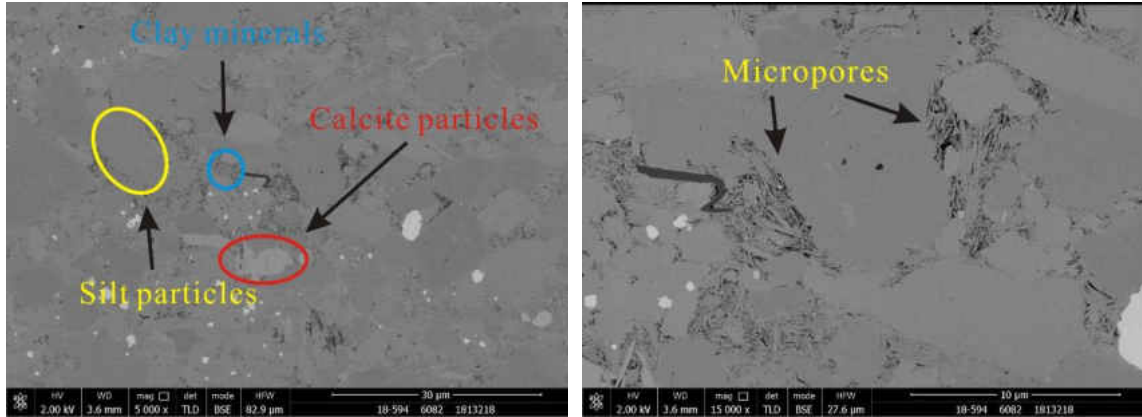
SEM can provide 2D images at a high level of magnification, which is useful for evaluating micritic porosity and other submicron feature (Bonnie et al., 1992). Argon Ion Polishing uses wide argon ion beam (<1mm) to polish the rock samples surface and remove the damaged layer, so that it can prepare a broad and precise area of electron microanalysis on samples for the SEM test (Clelland et al., 1991; Liu et al., 2011).

The SEM machine we used here is the Helios 650 Focused Ion Beam Scanning Electron Microscopy. We tested samples from three actual Bakken wells with the depth of the Middle Bakken layer. The lithology of rock samples from Well 1 can be defined as carbonaceous calcareous siltstone, as shown in **Fig. 4**.



(a) Organic matter content is very low (black part), a few micro fractures developed.

(b) A small number of micropores can find inside the organic matter



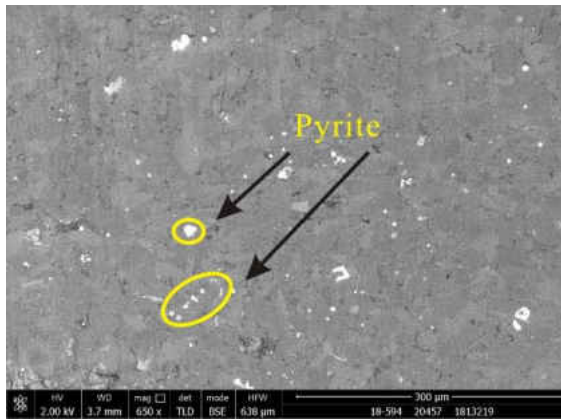
(c) Clay minerals distributed in the pores between silt particles and calcite particles

(d) Micropores well developed in the interlamellar clay minerals

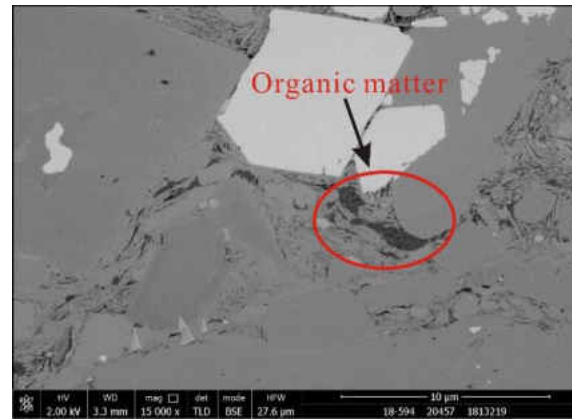
Fig. 4 Bakken rock sample SEM results of well 1.

According to the SEM results, the fracture is not well developed in this area, because we only found a small number of micro-fractures developed. For the sample's organic composition, the organic matter content is very low, these fine organic matter debris adhered to the surface of the sample and organic matter pores do not occur. Clay minerals distributed in the intergranular pores between silt particles and calcite particles, and the micropores of interlamellar clay minerals are well developed. A small number of microfractures developed in the silty sand particles.

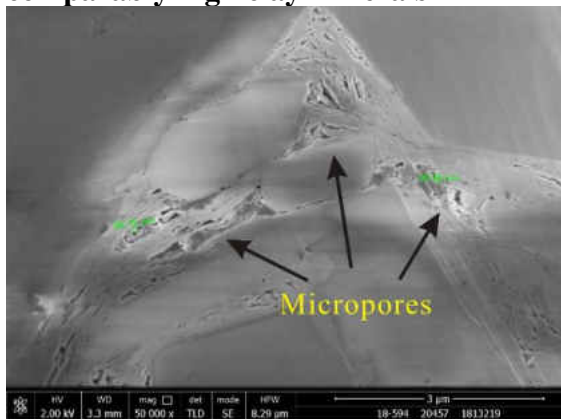
The SEM results show that the lithology of the rock in well 2 is silty mudstone. As shown in **Fig. 5**, the content of organic matter is also very low, a little organic matter distributed between clay minerals. Some organic matter has a small number of micropores developed. The interlamellar micropores of clay minerals are well developed, and it was found that some micropores are present in magnesite particles.



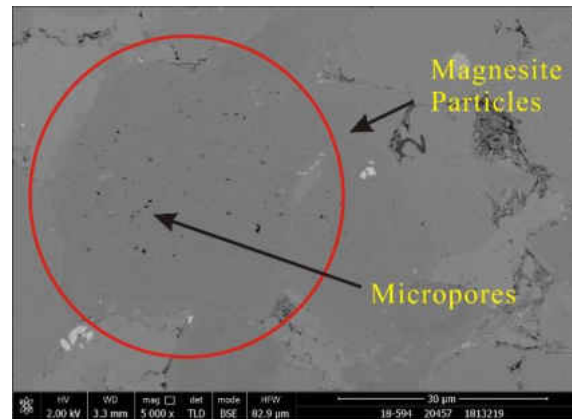
(a) Low organic matter content but comparably high clay minerals



(b) Organic matter fills the clay minerals



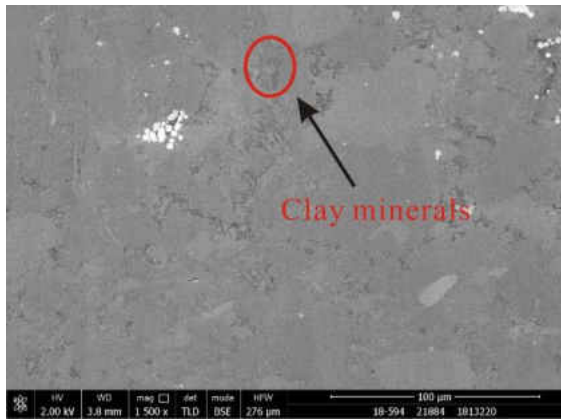
(c) Some micropores developed inside the organic matter



(d) A small number of micropores develop in magnesite particles

Fig. 5 SEM results of Bakken rock sample from well 2.

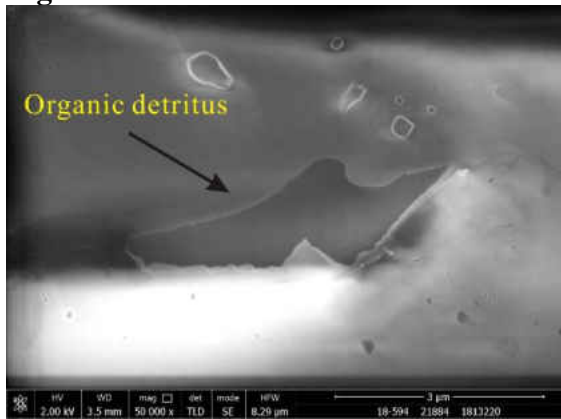
The lithology of rock type in Well 3 is the calcareous siltstone, as shown in **Fig. 6**. There are many clay minerals in the intergranular pores of silt and calcite. The content of organic matter is low, and only a few tiny organic matter fragments were found. The pores in the organic matter are not well developed. A small number of intracrystalline micropores generate in calcite.



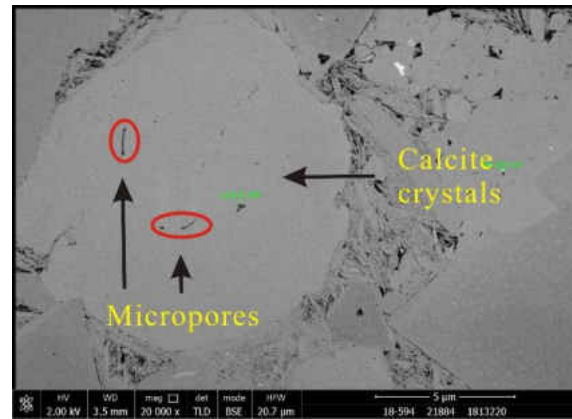
(a) Clay minerals in the intergranular pores of calcareous siltstone, low organic content



(b) Interlamellar micropores well developed in clay minerals



(c) Micropores in organic detritus are not well developed



(d) A small number of micropores present in calcite crystals

Fig. 6 Bakken rock sample SEM results of well 3.

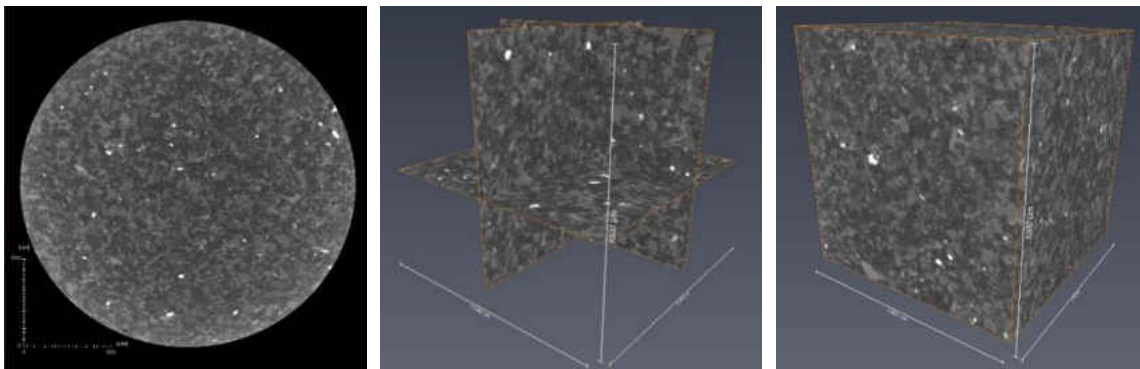
Base on the SEM results of three different wells form Middle Bakken formation, it was determined that the lithology of this area is calcareous siltstone or silty mudstone which can be characterized as a tight reservoir with low porosity and low permeability. The content of organic matter is low, so this layer is a reservoir in Bakken Formation. Micropores are not developed well in the organic matter, which in turn fully developed in interlamellar clay minerals. The microfractures hardly found in this area.

3.2 Computed Tomography (CT) Scans

CT Scans is an efficient way to test the porosity and structure of the rock sample. It can determine the porosity and pore space morphology, therefore to predict the permeability and porosity properties of rock samples. Some samples have defects (chipping, fractures), which are impossible for standard laboratory tests to be detected, but the CT scans can give a better understanding of rock samples. Moreover, also some samples are hard-to-recover or fundamental analyses are significantly time-consuming. Those types of samples can be easily handled with CT scans. A 3D analysis of porosity, mineral distribution, shape and morphometries can be attained after the CT scans.

The principle of this test is using the recreation of X-ray binary models in three-dimensional images (Vakhrusheva et al., 2015). The sample is placed inside the scanner, and the core holder will rotate with the sample during the X-ray beam scanning, leaving the shadow projection (a separate two-dimensional image corresponding to the X-ray intensity passing through the sample) on the detector (camera) (Ponomarev et al., 2016).

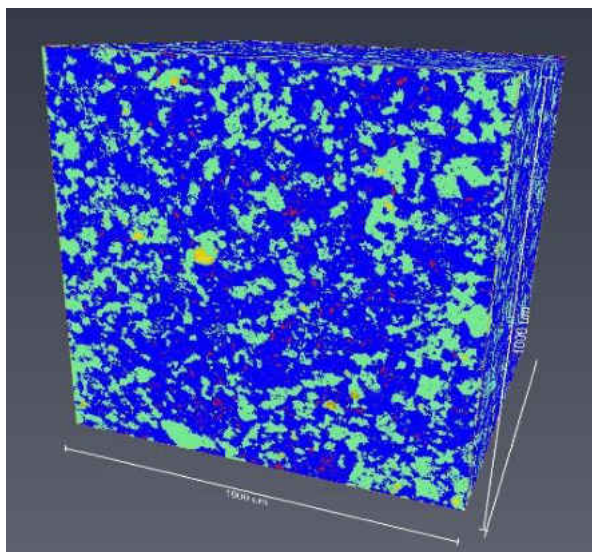
The results of the CT scans were used to reconstruct the digital rock sample model, as shown in **Fig. 7**.



(a) Core section (2mm)

(b) Section diagrams in three directions

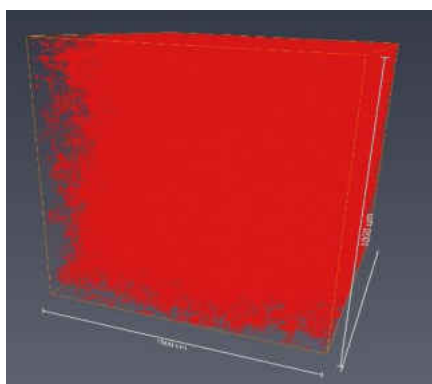
(c) Three-dimensional reconstruction



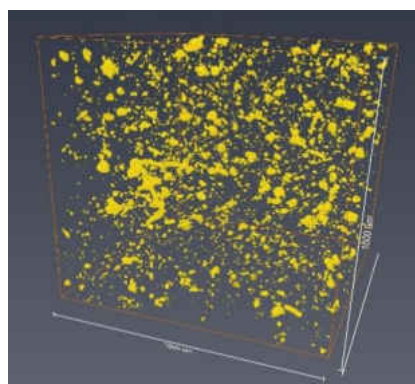
(d) Mineral and pores distribution reconstruction (1000 μm *1000 μm *1000 μm) after threshold segmentation with pores (red), siliceous or argillaceous (blue), calcareous (green) and heavy mineral (yellow).

Fig. 7 Steps of a 3D model reconstruction for the middle Bakken rock sample through CT scans method (from a to d).

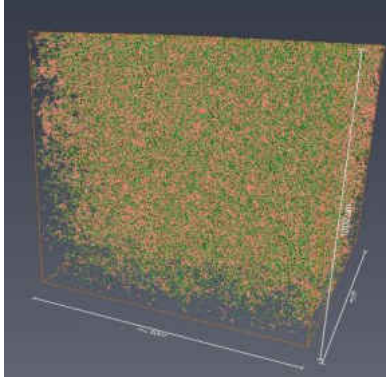
According to the phase diagram, the rock model was divided into four models which keep the original model size and shape but presented different rock properties such as pores, heavy minerals, and pore throats as shown in **Fig. 8**.



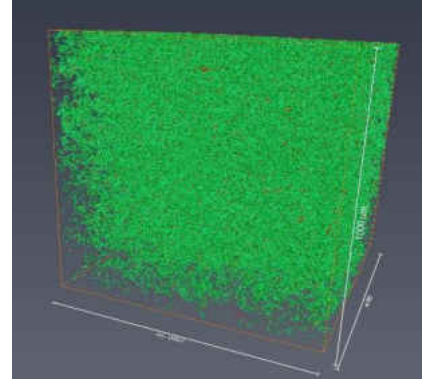
(a) Pore distribution characteristics



(b) Heavy minerals distribution characteristics



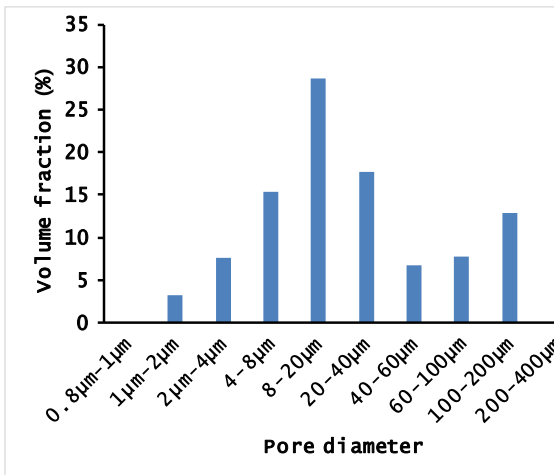
(c) Pore throat distribution characteristic, the pore is in green and pore throat is in pink



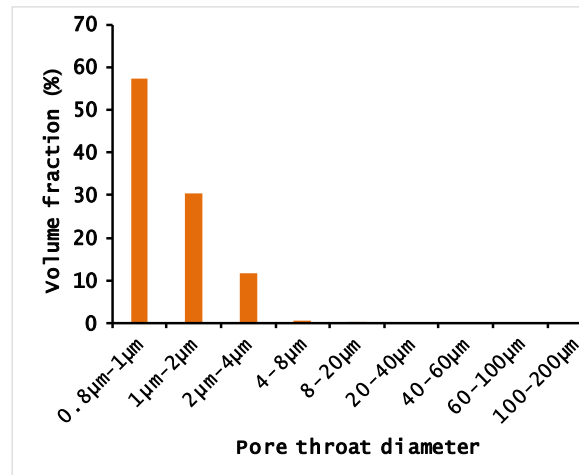
(d) Pore throat distribution characteristics, red points represent the best connectivity

Fig. 8 Different rock properties distribution characterization of the Middle Bakken rock sample through CT scans.

The data of the Avizo digital core processing results summarized in **Fig. 9**. Two diagrams attached which are pore distribution diagram (left) and pore throat distribution diagram (right). These diagrams concluded from 1,000,000 data points analyzed by the Avizo digital core processing. Therefore, the results got there based on big data. In this case, we believe the data is comparably accurate.



(a) Pore distribution diagram



(b) Pore throat distribution diagram

Fig. 9 Quantization of the pore distribution and pore throat distribution.

According to these two diagrams, it is clear to see that the pore diameter mainly distributed in the range from 4 μm to 40 μm . The pore throat diameter is between 0.8~2 μm . We compared the data from CT scans using Avizo digital rock processing, and found that the porosity is 4%, the porosity is low. Siliceous and argillaceous volume fraction is 64.8%, calcareous volume fraction is 30.9%, and heavy minerals volume fraction are 0.3%. The minimum pore throat diameter is 1 μm , the maximum pore throat diameter is 11.3 μm , average pore throat diameter is 1.02 μm , and average pore throat length is 7.45 μm . The pore throat is also low, indicates low permeability in this layer. This Avizo digital rock processing confirmed this layer is tight oil reservoir with low permeability, and low porosity. The summarization of the CT scans experiments and Avizo digital rock processing listed in **Table 1**.

Table 1. Middle Bakken rock sample analysis by Avizo digital rock processing.

Parameter	Value
Pore volume (%)	4
Siliceous, argillaceous (%)	64.8
Calcareous (%)	30.9
Heavy minerals (%)	0.3
Min pore throat diameter (μm)	1
Max pore throat diameter (μm)	11.3
Ave pore throat diameter (μm)	1.02
Ave pore throat length (μm)	7.45

3.3 Thin Section Petrography

The microscope is widely used in thin section petrography to distinguish the lithology of rock from the reservoir. The magnification and accuracy are important for the microscope. They are the crucial factors to consider before the microscope examination (Bi et al., 2018). The metallurgical microscope has excellent magnification and resolution compared with

other microscopes. Various filters are available to use and have a wide range of observation (Song et al., 2002).

Metallurgical microscopes equipped with an incident light source which sends the light through the objective onto the reflective surface of the metal. The sample should be polished to have a perfectly flat surface. The metallurgical microscope system can connect the traditional optical microscope to the computer (digital camera) through the photoelectric conversion of organic unifies in together. This kind of microscope can not only make the microscopic observation on the eyepiece, but also observe the real-time dynamic display screen images in the computer (digital camera). It can edit, save and print photos.

Therefore, IMAGER. A2M metallurgical microscope was used in this study to discover the lithological properties of the three rock samples from the Middle Bakken Formation. These three rock samples are from the same three wells we mentioned before. These rock samples are got from the corresponding well numbers.



(a) Thin section photo in the metallurgical microscope



(b) The fluorescent light source

(c) Polarized light source

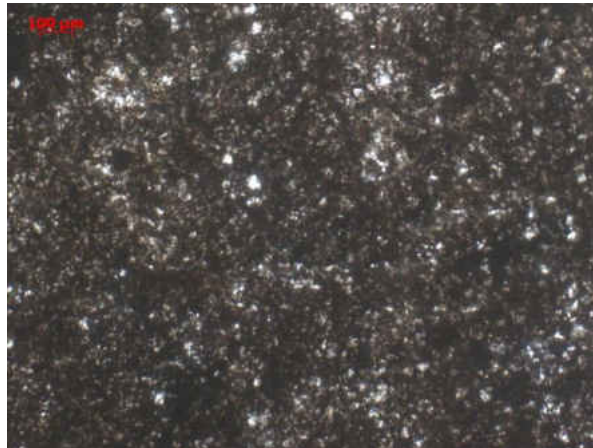
Fig. 10 Metallurgical microscope results of thin section observation under different light sources (well 1).

As shown in **Fig. 10**, the metallurgical microscope results showed that the lithology of this rock is micritic marly dolomite contains stucco cloud in grain structure and argillaceous structure. The rock is mainly composed of carbonate minerals mixed with argillaceous materials, and the silt clastics distributed in star point shape. A small amount of pyrite (about 3%) distributed between the crystals in irregular or patch shape.

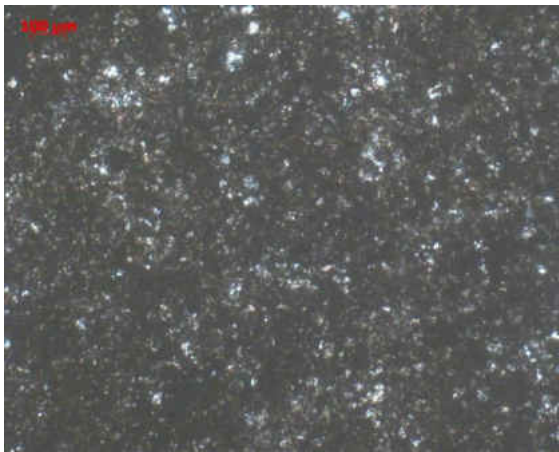
Carbonate minerals are mainly powder-micritic dolomite with a few calcites which is distributed between the grains in the form of pores. The clay minerals are cryptocrystalline and distributed unevenly. Micrite dolomite is poor in the color of black light due to mixed with argillaceous. A little powder crystal dolomite has a higher degree of automorphism. Silt clastics are mainly quartz and feldspar in the shape of subcircular – prismatic, particle size is more extensive than 0.03mm.

In the rock slice, there were a few sporadically distributed bits of bioclastic particles, some of which were larger than others. The grains were recrystallized and composed of calcite which was mainly composed of mosses, shell and brachiopods. So the content of this thin

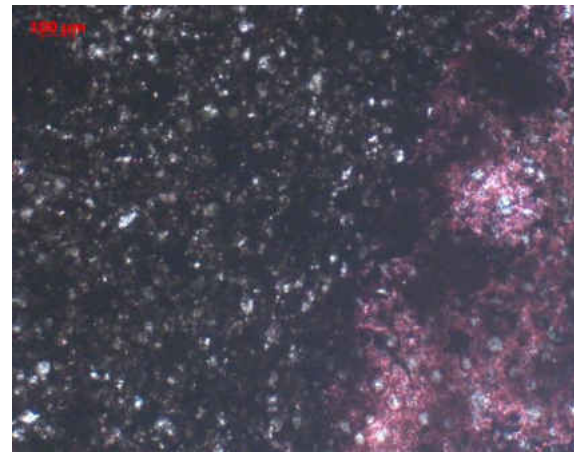
section can be presented as dolomite and clay mineral occupied 73 %, calcite occupied 20% and silty clastic accounted for 7%.



(a) Thin section photo in the metallurgical microscope



(b) The fluorescent light source



(c) Polarized light source

Fig. 11 Metallurgical microscope results of thin section observation under different light sources (well 2).

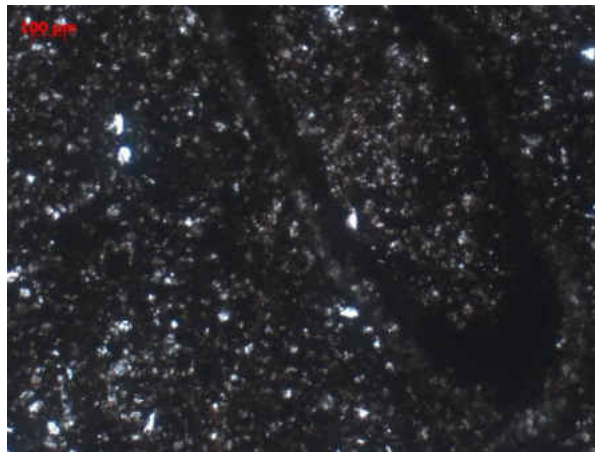
Fig. 11 shows the images from the metallurgical microscope. This rock two can also be defined as micritic marly dolomite containing stucco cloud in grain structure and argillaceous structure. The rock is mainly composed of carbonate minerals mixed with

argillaceous materials, and the star points of silt clastics distributed in it. A little bit of yellow iron (about 6%) was patchy in the intergranular and locally abundant.

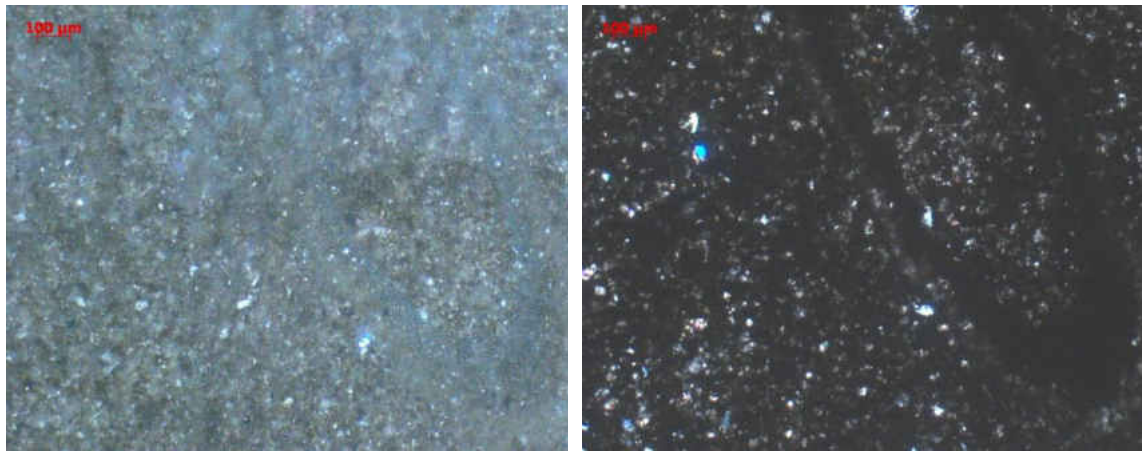
Carbonate minerals are mainly powder-micritic dolomite with a few cubic stones. Micrite dolomite mixed with argillaceous shows poor color in black light. A little powder crystal dolomite is in high degree of automorphism. Calcite distributed between the grains in the form of pores, and some enriched in patch shape. Silt clastics are mainly quartz and feldspar with a subcircular – prismatic shape, the particle size is smaller than 0.06mm.

Flocculent and lumpy particles were more concentrated in the rock slices. It is mainly composed of carbonate minerals, which may derived from granular alteration, such as algae.

The content of the rock can be defined as dolomite and clay mineral is 75%, calcite is 20% and silt clastic is 5%.



(a) Thin section photo in the metallurgical microscope



(b) The fluorescent light source

(c) Polarized light source

Fig. 12 Metallurgical microscope results of thin section observation under different light sources (well 3).

Fig. 12 is the results of metallurgical microscope analysis of samples 3. It is a black dolomite mudstone in grain structure and argillaceous structure. The rock is mainly composed of clay minerals mixed with black minerals and carbonate minerals, and the silt clastics distributed in star points. A small amount of pyrite (about 7%) is speckled, irregular, curved and banded distributed in intercrystalline form. Clay minerals are cryptocrystalline, mostly mixed with black minerals, and distributed in dense clumps. Carbonate minerals are mainly powder-micritic dolomite with a few calcite pores unevenly distributed among the crystals. Silt clastics are mainly quartz, and feldspar with subcircular - prismatic and particle size are smaller than 0.06mm. Shell-like particles are uncommon to see. The granular crust is mainly composed of black mineral mixed clay.

The composition of the rock can be defined as clay mineral, black mineral and dolomite in 79%, calcite in 15% and silt detritus in 6%.

According to the metallurgical microscope results, the lithology of this area is mainly dolomite and mudstone. The rock is mainly composed of dolomite and clay mineral, a part

of calcite and a little silt detritus. Comparably good roundness of the particle and the particle size are smaller than 0.06mm but larger than 0.03mm. The structure of the particles is mainly grain structure and argillaceous structure.

CHAPTER VI

RESERVOIR SIMULATION OF FIELD SCALE CO₂ HUFF-N-PUFF PROCESS

4.1 Description of the Simulation Model

The Peng-Robinson equation of state (PR-EOS) model is the principle method used in CMG-GEM compositional simulation for phase equilibrium calculation. CO₂ molecular diffusion coefficient will directly affect the penetration depth and injection gas saturation distribution in the reservoir.

PR-EOS model is a typically basic model used in petroleum industries. In this case, we describe the phase behavior of solvent(s)-CO₂ oil systems using this PR-EOS model as the equation of state. The PR-EOS model (Peng and Robinson, 1976) can be expressed as:

$$P = \frac{RT}{V-b} - \frac{a}{V(V+b)+b(V-b)} \quad (1)$$

$$a = a_c \alpha(T_r, \omega) \quad (2)$$

$$a_c = \frac{0.457235R^2T_c^2}{P_c} \quad (3)$$

and

$$b = \frac{0.0777969RT_c}{P_c} \quad (4)$$

where $\alpha(T_r, \omega)$ is the alpha function that correlates with reduced temperature T_r and acentric factor ω , V is molar volume, R is the universal gas constant, P_c is critical pressure and T_c is critical temperature. The Soave-type alpha function used in the PR-EOS model is given by Peng and Robinson (1976):

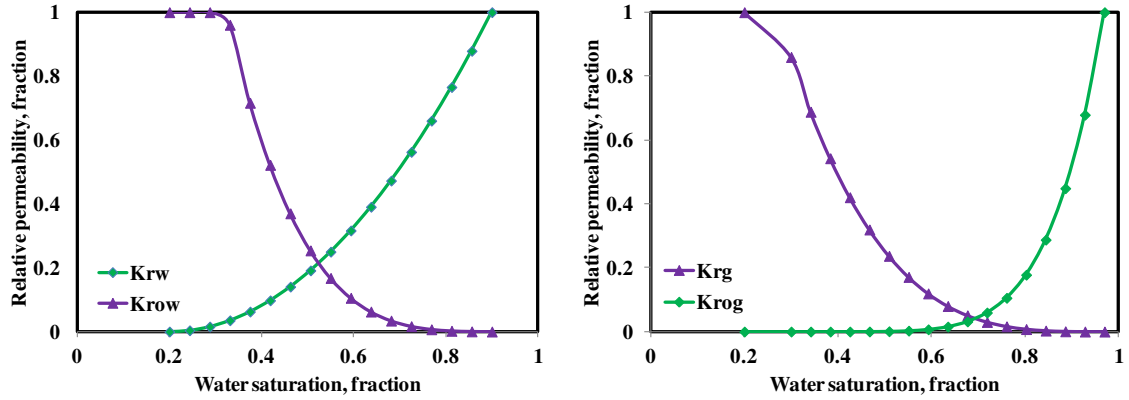
$$\alpha = [1 + (0.37469 + 1.54226\omega - 0.26992\omega^2)(1 - T_r^{0.5})]^2 \quad (5)$$

Given the effective range of Middle Bakken reservoir properties, the Middle Bakken reservoir model with multi-stage hydraulic fractures was built according to one actual well in Middle Bakken formation. The boundary condition in this model is assumed as the no-flow boundary condition. The specific data of the reservoir and hydraulic fractures are listed in **Table 2**.

Table 2. Field case reservoir model parameters.

Parameter	Value	Unit
Model dimension (x×y×z)	10502×2640.2×50	ft
Number of gridblocks (x×y×z)	181×42×1	-
Initial reservoir pressure	7800	psi
Reservoir temperature	240	°F
Reservoir permeability	0.02	mD
Reservoir porosity	5.6%	-
Initial water saturation	40%	-
Total compressibility	1×10 ⁻⁶	psi ⁻¹
Reservoir thickness	50	ft
Well length	8555	ft
Number of stages	15	-
Clusters per stage	2	-
Cluster spacing	354	ft
Fracture half-length	92.1	ft
Fracture height	50	ft
Fracture width	0.01	ft
Fracture conductivity	500	md-ft

For the rock-fluid part, the relative permeability curves of water-oil relative permeability and liquid-gas relative permeability are shown in **Fig. 13**. Only one set of relative permeability curves were used for all the grid, and the non-Darcy effect is not considered.



(a) Water-oil relative permeability curve (b) Liquid-gas relative permeability curve

Fig. 13 Relative permeability curves used in this study (Yu et al., 2014).

4.2 Fluid Model

On account of the problem that the detailed fluid characterization data in this Middle Bakken well is not available, CMG-Winprop was used to generate the fluid model on the basis of crude oil properties in the Middle Bakken reservoir. Seven pseudo-components were assumed in this study, i.e., CO_2 , N_2-C_1 , C_2-C_4 , C_5-C_7 , C_8-C_{12} , $C_{13}-C_{19}$, C_{20+} . The corresponding molar fractions are 0.0118, 0.0016, 0.2454, 0.2445, 0.1892, 0.2215 and 0.086, respectively. More detailed data required for the Peng-Robinson equation-of-state are listed in **Table 3**. **Table 4** lists the binary interaction parameters which are used for phase behavior calculation. In summary of the fluid property, the bubble point pressure is 2501.253 psia, API gravity of crude oil is 42°, the gas oil ratio (GOR) is 853.04 scf/stb, formation volume factor (FVF) is 1.505 and the minimum miscible pressure (MMP) is 3260 psia.

Table 3. Compositional data for the Middle Bakken formation.

Component	Molar fraction	Critical pressure (atm)	Critical temperature (K)	Critical volume (L/mol)	Molar weight (g/gmol)	Acentric factor	Parachor coefficient
CO2	0.0118	72.80	304.20	0.0940	44.01	0.2250	78.0
N2	0.0016	33.50	126.20	0.0895	28.01	0.0400	41.0
CH4	0.2454	45.40	190.60	0.0990	16.04	0.0080	77.0
C2HtoNC4	0.2445	41.92	371.46	0.2039	44.79	0.1481	150.5
IC5toC07	0.1892	33.11	506.94	0.3367	83.87	0.2526	249.7
C08toC12	0.2215	27.91	709.72	0.4567	120.54	0.3294	345.2
C13toC30	0.0860	20.73	986.86	0.9700	297.27	0.7532	736.6

Table 4. Binary interaction parameters for Middle Bakken oil.

	CO ₂	N ₂	C ₁	C ₂ -C ₄	C ₅ -C ₇	C ₈ -C ₁₂	C ₁₃₊
CO ₂	0	-0.0200	0.1030	0.1317	0.1420	0.1463	0.1645
N ₂	-0.0200	0	0.0310	0.0773	0.1120	0.1200	0.1200
C ₁	0.1030	0.0310	0	0	0	0	0
C ₂ -C ₄	0.1317	0.0773	0	0	0	0	0
C ₅ -C ₇	0.1420	0.1120	0	0	0	0	0
C ₈ -C ₁₂	0.1463	0.1200	0	0	0	0	0
C ₁₃₊	0.1645	0.1200	0	0	0	0	0

4.3 EDFM Validation

Any complex fractures can be modelled using EDFM method through the structured gridding method. It is definitely simple but effective (Moinfar et al., 2014; Xu, 2015). In this method, mass transfer can be calculated through some fracture grids which are in contact with corresponding matrix grids. According to the matrix-grid boundaries, each fracture could be discretized into several fracture segments. Some fluid transport between fractures, matrix, and well can be simulated inside the reservoir simulators using non-neighboring connections (NNCs) and effective wellbore index as:

$$T_{NNC} = \frac{K_{NNC}A_{NNC}}{d_{NNC}} \quad (6)$$

where T_{NNC} is the transmissibility factor, K_{NNC} is matrix permeability for the fracture-matrix connection and also average fracture permeability for the fracture-fracture connection,

A_{NNC} is the contact area between the NNC pair, and d_{NNC} is the average distance between the NNC pair.

For the fracture-well connection, the modified Peaceman's model is used to calculate the wellbore index:

$$WI_f = \frac{2\pi k_f w_f}{\ln(r_e/r_w)} \quad (7)$$

$$r_e = 0.14\sqrt{L^2 + W^2} \quad (8)$$

where w_f is the fracture width, k_f is the fracture permeability, L is the fracture-segment length, and W is the fracture-segment height (Xu et al. 2017a, 2017b).

EDFM, as shown in **Fig. 14(a)**, only embed fracture into a matrix grid directly. The profit of this method is that the refined grid will not require to be created or even calculated during the simulation. As a contrast, the LGR method as shown in **Fig. 14(b)**, will inevitably create some refined grids near the fractures. In this case, the total amount of grids for the EDFM method will be less than the LGR method, so that it will take less CPU time to run a simulation.

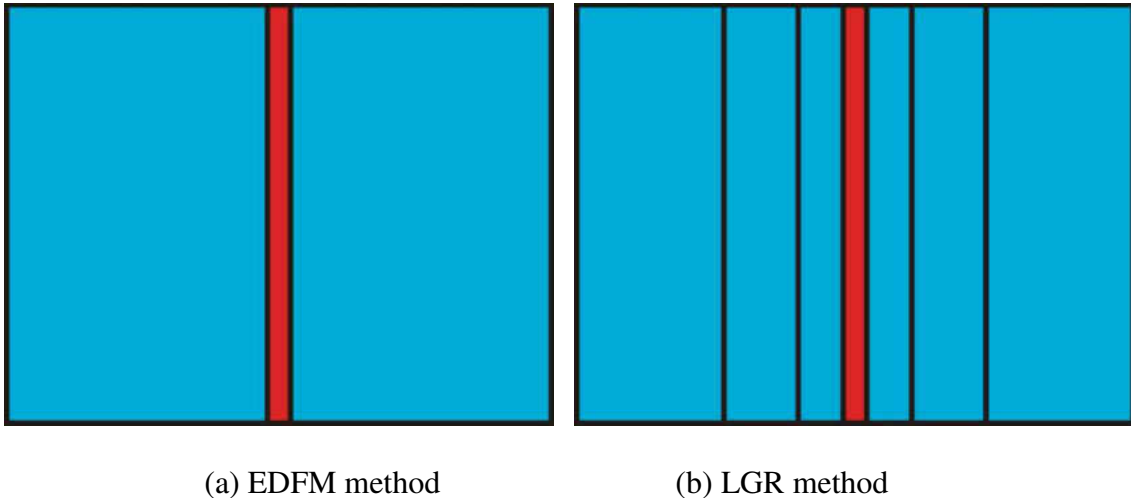
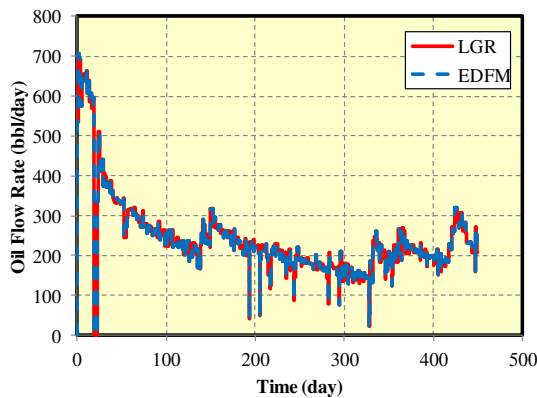


Fig. 14 Comparison of fracture modelling between EDFM and LGR.

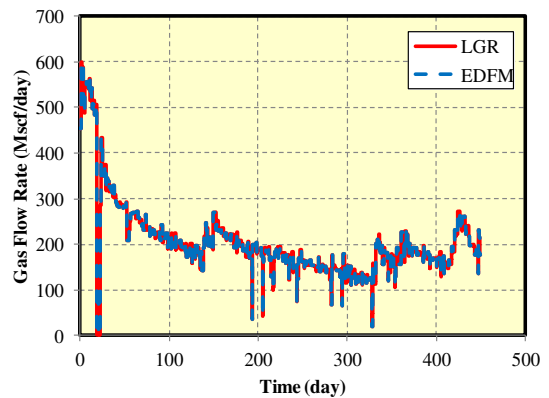
Given the fact that the EDFM method is a new fracture modelling method, the accuracy of this method needs to be verified before conducting any case study. Therefore, we compared the EDFM method and the LGR method by running the same case, which we got from the real field history data. Under the same circumstances, we can compare the simulation results to find out the accuracy of the EDFM method.

The difference between these two models is only the grid used to create the fractures. One of these two models used EDFM method to create the fracture grids. In the other case, the LGR method was used to create the fracture grids, where each matrix grid containing fracture set as $9 \times 1 \times 1$.

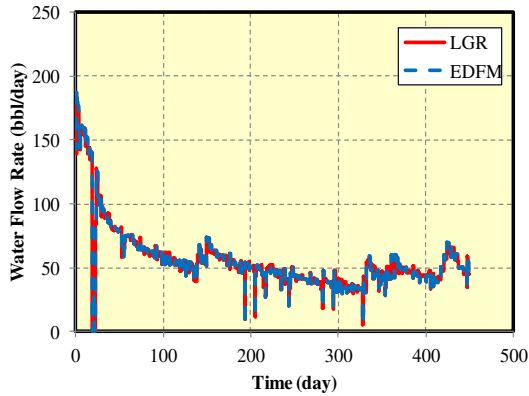
We compared these two simulation results on oil production rate, gas production rate, water production rate and bottomhole pressure under the same well constraint condition after running the same production time. As shown in **Fig. 15**, an excellent agreement was achieved between EDFM and LGR. Therefore, it was verified that the EDFM method has the same accuracy as the LGR method to simulate the reservoir property and predict further production.



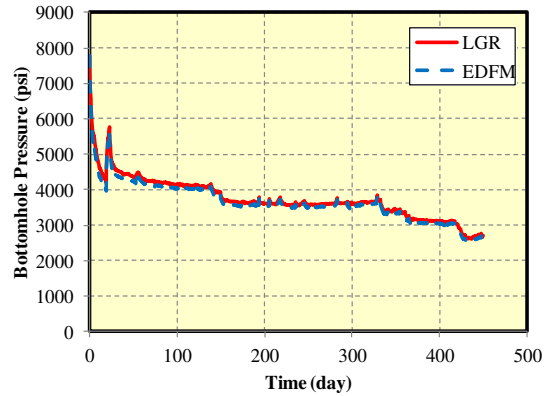
(a) Oil flow rate



(b) Gas flow rate



(c) Water flow rate



(d) Bottomhole pressure

Fig. 15 Comparison of well performance and BHP between LGR and EDFM.

Besides, while the EDFM and LGR have the same accuracy, the EDFM method provides significant computational efficiency. The EDFM method can save about 45% CPU time comparing with the LGR method. In this case, we used the EDFM method to continue our following simulation case studies.

4.4 History Match

Before conducting the simulation case study of sensitivity factor, it is imperative to verify the reliability of the simulation model. An actual well with 451 days' production data from the Middle Bakken was selected to perform history matching (Kurtoglu and Kazemi, 2012). A field-scale reservoir model was developed in a commercial simulator combining with EDFM software to simulate CO₂ Huff-n-Puff experiment. Thirty bi-wing hydraulic fractures were set in the model. A horizontal well penetrates all of the fractures in the middle position. The model dimension is 10502 ft × 2640.2 ft × 50 ft, which corresponds to length, width and height, respectively, as shown in **Fig. 16**.

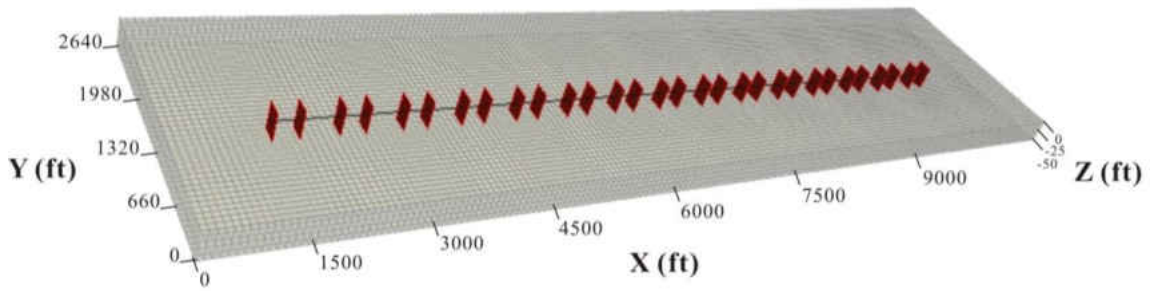


Fig. 16 A field-scale reservoir model with one horizontal well penetrated 30 bi-wing hydraulic fractures.

In our history matching simulation, the oil rate measured from the field was used as constraint, as shown in **Fig. 17**. Gas rate and bottomhole pressure (BHP) are the target parameters for history matching. Fracture half-length, fracture conductivity, and matrix permeability were the main the tuning parameters to achieve good match results.

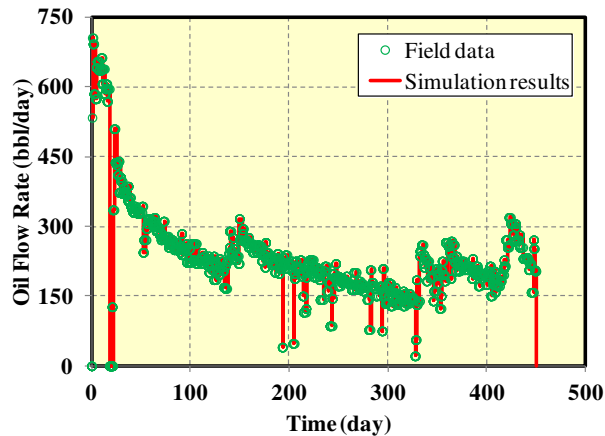
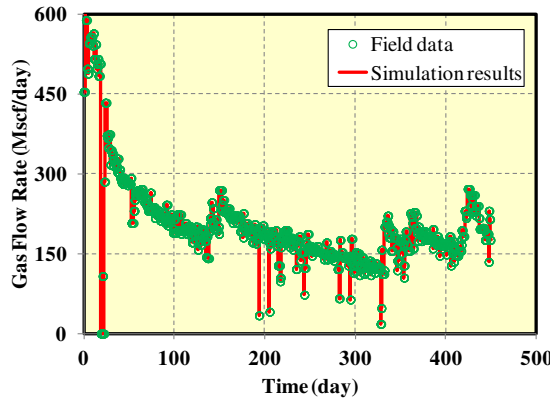
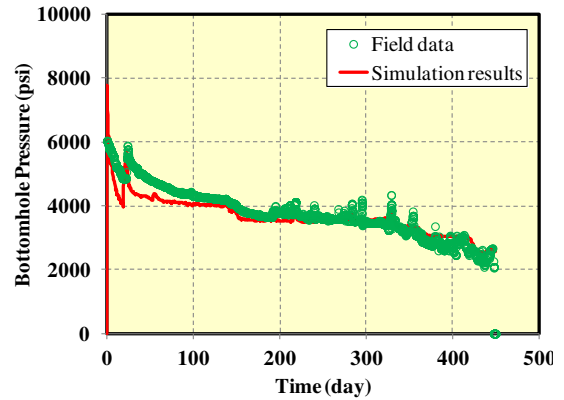


Fig. 17 Oil flow rate comparison between the actual well data and simulation results.

As shown in **Fig. 18(a)** and **Fig. 18(b)**, a great match between the simulation results and actual field production data in gas rate and bottomhole pressure was achieved. Based on the excellent history match, the fracture conductivity is 500 md-ft, fracture half-length is 92.1 ft, and matrix permeability is 0.02 md.



(a) Gas flow rate



(b) Bottomhole pressure

Fig. 18 Comparison of gas flow rate and bottomhole pressure between real well production data and simulation model results.

After running 451 days of actual production date, the simulation results (**Fig. 19**) showed that the pressure drop in grids close to hydraulic fractures were much higher comparing with pressure in the grids far away from the hydraulic fractures. This phenomenon indicates a reasonable oil recovery process that the oil was produced from the reservoir to the surface, through the fractures to the well.

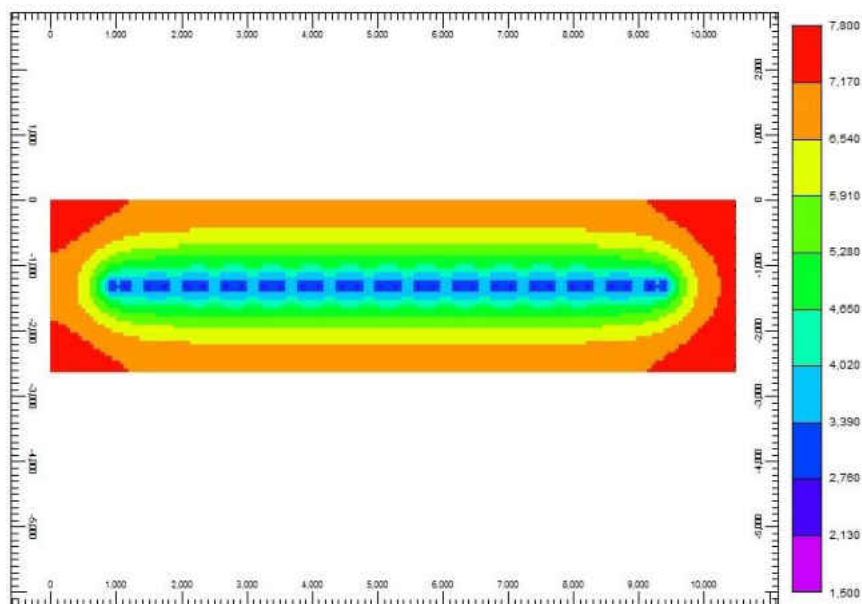


Fig. 19 Pressure distribution at the end of the history match.

Given it is time-consuming to continue our case studies in a field case with 30 hydraulic fractures, our study chose a small part of the field case model to continue our CO₂ Huff-n-Puff study. As shown in **Fig. 20**, there is only one stimulation stage with two bi-wing hydraulic fractures set in our section model. The detailed parameters input for our model as listed in **Table 5**. The fracture conductivity, fracture half-length, and so on, are the same as the field case model.

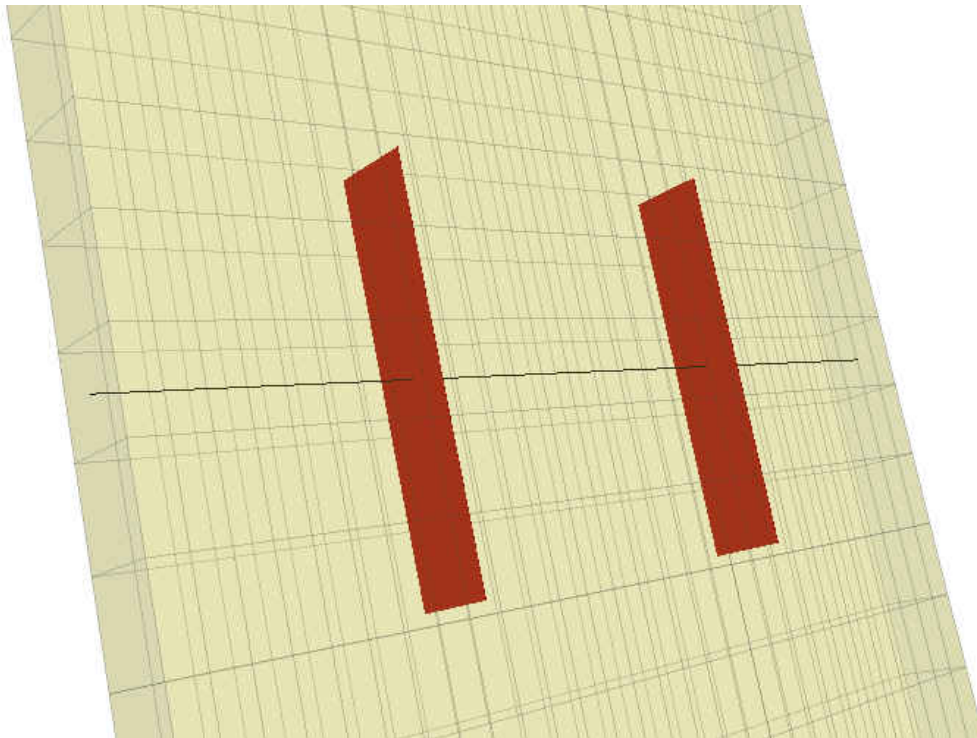


Fig. 20 A section model with a horizontal well and 2 bi-wing hydraulic fractures.

Table 5. Section history matching parameters.

Parameter	Value	Unit
Model dimension (x×y×z)	580×2150×50	ft
Number of gridblocks (x×y×z)	30×43×1	-
Initial reservoir pressure	7800	psi
Reservoir temperature	240	°F
Reservoir permeability	0.02	mD
Reservoir porosity	5.6%	-
Initial water saturation	40%	-
Total compressibility	1×10^{-6}	psi ⁻¹
Reservoir thickness	50	ft
Well length	578.8	ft
Stage spacing	236	ft
Fracture half-length	92.1	ft
Fracture height	50	ft
Fracture width	0.01	ft
Fracture conductivity	500	md-ft

The well constraint also set the oil rate according to the actual well production data. Hence, the fractures and field dimensions are 15 times smaller than the actual field model. The actual well performance will also be divided by 15, as shown in **Fig. 21**.

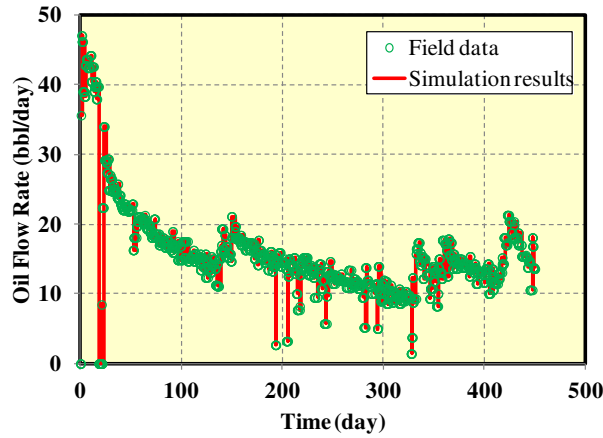


Fig. 21 Oil flow rate comparison between actual well data and section model results.

For the gas flow rate and bottomhole pressure parameters, an excellent history match is also achieved in this section model, as shown in **Fig. 22**. The pressure distribution is shown in **Fig. 23**, the same effect as the field model can be found in this figure.

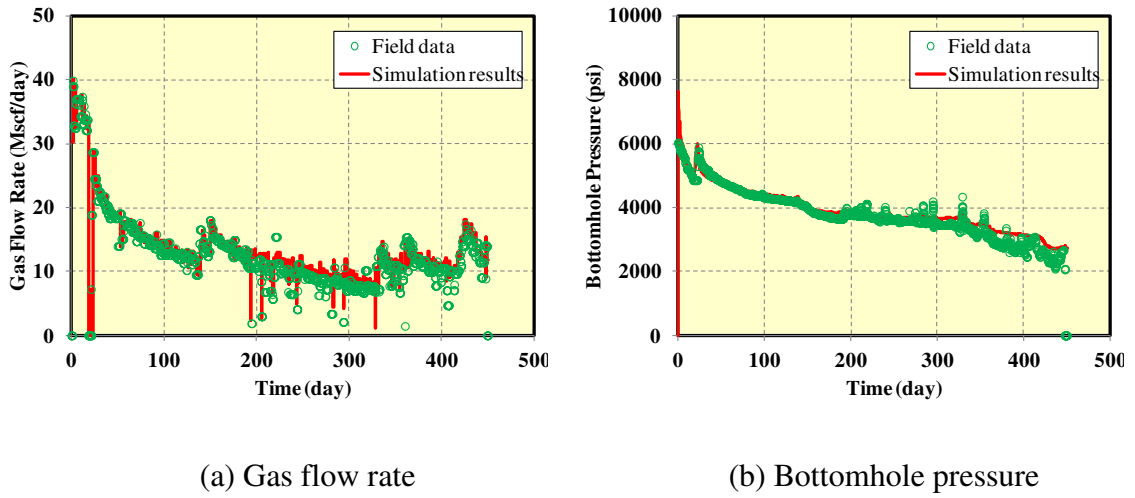


Fig. 22 Comparison of gas flow rate and bottomhole pressure between modified well production data and simulation model results.

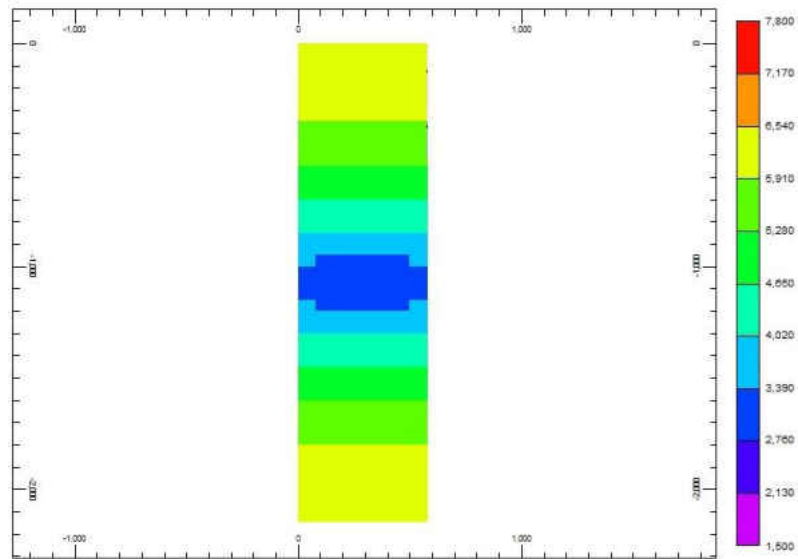


Fig. 23 Section Model pressure distribution at the end of the history match.

4.5 Sensitivity Analysis

Five scenarios were designed in this study to investigate the Huff-n-Puff effects on CO₂ EOR in the Middle Bakken. There is only one variable parameter in each scenario according to the base case. The scope of variable parameters is all in the reasonable range based on the literature review. The five variable parameters are CO₂ injection rate, CO₂ injection time, soaking time, numbers of CO₂ Huff-n-Puff cycle and CO₂ diffusion coefficient.

The base case we used in this study has a total of 7000 production days, with three cycles of CO₂ Huff-n-Puff. After the history matching period, the production well was set to shut-in at 500th day. At the same time, the injection well will inject CO₂ in the rate of 200 Mscf/day for 50 days, and then close the injection well for a 14 days' soaking period. The minimum bottomhole pressure set at a constant value of 1500 psi as a constraint of the production well. It is the first CO₂ Huff-n-Puff cycle. The second and the third cycle will be conducted at 2500th day and 4500th day, with the same injection rate, injection time and soaking time. The CO₂ diffusion coefficient used in this base case is 0.005 cm²/s.

Effect of CO₂ injection rate.

Three cases, including the base case, were conducted in this scenario to compare the oil recovery factor with the primary production. The CO₂ injection rate was modified to 50 Mscf/day and 350 Mscf/day and other parameters were not changed. As shown in **Fig. 24**, after the history matching period, the cumulative oil production without CO₂ injection (Primary production) keep the highest cumulative oil recovery, followed by the case with a CO₂ injection rate of 50 Mscf/day, 200 Mscf/day and 350 Mscf/day in sequence. At the

time of 1000th day, which is the middle of the first cycle, the cumulative oil production of three cases was going closed and almost at the same level compared with primary production. After 1000 days, the case with high CO₂ injection rate becomes the highest cumulative production oil case, followed by other lower CO₂ injection rate in sequence. At the end of the simulation, cumulative oil production of the case with 200 Mscf/day CO₂ injection rate is close to that of 350 Mscf/day CO₂ injection rate, but much higher than the case with 50 Mscf/day CO₂ injection rate. The contribution to cumulative oil production after 7000 days is about 1.3%, 3.2% and 3.4% for the three CO₂ Huff-n-Puff cases with the CO₂ injection rate of 50, 200 and 350 Mscf/day, respectively. Moreover, all of these cases with CO₂ injection have a higher cumulative oil production than the primary production. It means that CO₂ injection is beneficial for EOR, and with more CO₂ injected, the effect of CO₂ Huff-n-Puff will be stronger.

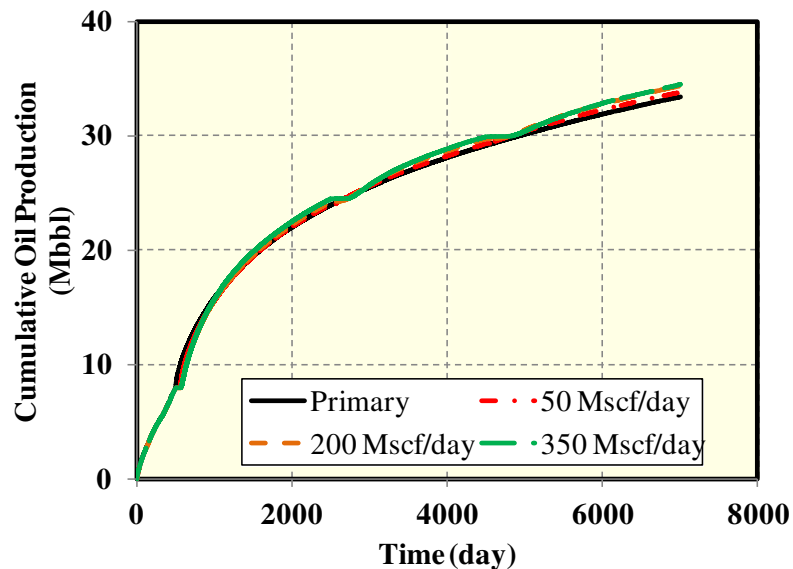
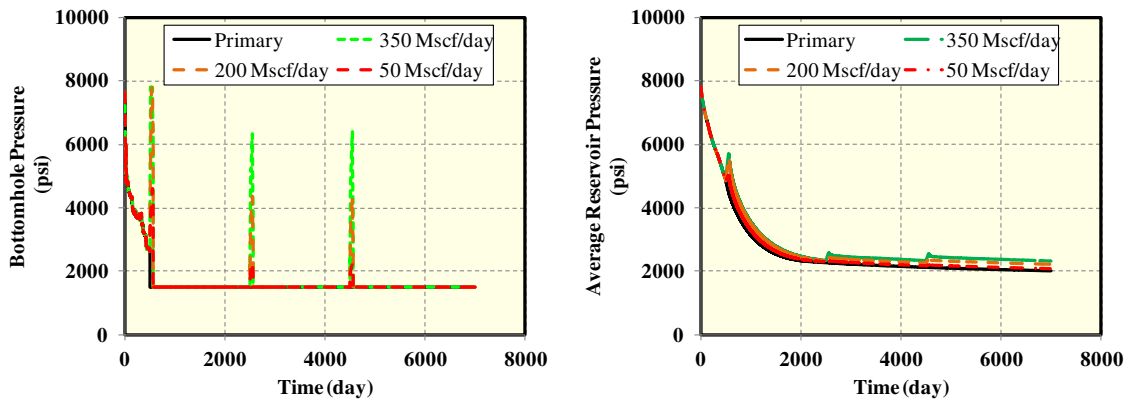


Fig. 24 Effect of different CO₂ injection rates on CO₂ Huff-n-Puff effectiveness.

According to the diagrams representing the well BHP and average reservoir pressure, we find the higher CO₂ injection rate corresponds to higher well BHP pressure and average reservoir pressure. The maximum bottomhole pressure was set as same as the initial pressure, which is 7800 psi. As the BHP reaches this limit, the injection rate will decrease automatically to keep the bottomhole pressure of 7800 psi. The case with higher CO₂ injection rate will reach the threshold much quicker than lower CO₂ injection rate one, as shown in **Fig. 25(a)**. Also, the higher BHP will transmit to the area nears the wellbore, and then transmits to other areas far away from the wellbore. Therefore, it is easier to lift the average reservoir pressure, as shown in **Fig. 25(b)**. With the high average reservoir pressure, the pressure difference helps accelerate the fluid flow from a high-pressure area (the reservoir) to low-pressure area (wellbore) during the production period.



(a) Bottomhole pressure

(b) Average reservoir pressure

Fig. 25 Effect of different CO₂ injection rate on wellbore and reservoir pressure.

Effect of CO₂ injection time.

In this CO₂ injection time study, two more modified case studies were conducted besides the base case. The CO₂ injection time modified from the base case, which is 50 days/stage,

to 10 days/stage and 100 days/stage. Other parameters were kept as same for three cases. The primary oil recovery was set as the control group. As shown in **Fig. 26**, after the history match, the case with 100 days/stage CO₂ injection time has the highest cumulative oil production compared with other cases. It is followed by 50 days/stage CO₂ injection time, 10 days/stage CO₂ injection time and the lowest one is primary production. The contribution to cumulative oil production after 7000 days is about 1.6%, 3.2% and 3.9% for the three CO₂ Huff-n-Puff cases with a CO₂ injection time of 10, 50 and 100 days, respectively. Comparing these four cases, the cumulative oil production with 100 days/stage is the lowest one at the beginning of each cycle due to the longer injection time without oil production. However, it surpasses other cases soon after the well starts to produce oil. The higher oil production rate helps the well production of this case not only catch up with other cases but also exceed them. It denotes that higher CO₂ injection time will lead to higher oil production rate. The difference in cumulative oil production between 10 days/stage, 50 days/stage and 100 days/stage is similar. Therefore, it is clear that higher injection time is beneficial for higher cumulative oil production, and this effect will proportionately increase. Meanwhile, in a given number of years, it is crucial to design an optimum ratio between injection time and production time according to the net present value (NPV) considered by the oil company.

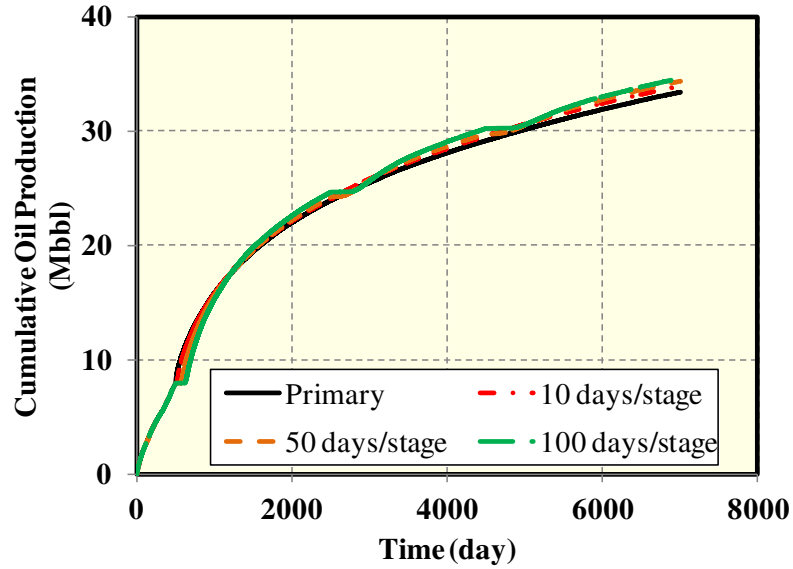
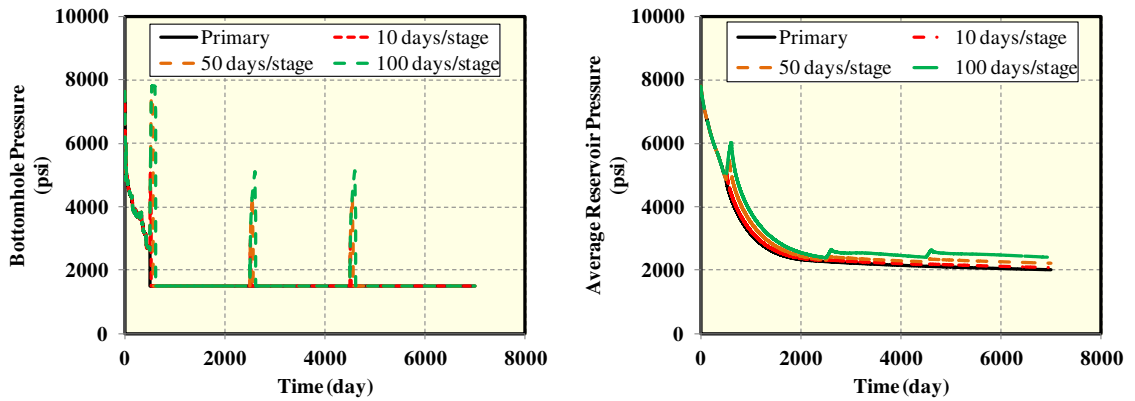


Fig. 26 Effect of different CO₂ injection time on CO₂ Huff-n-Puff effectiveness.

The essential issue that higher injection time will lead to higher oil production rate. As shown in **Fig. 27(a)**, the BHP of the case with 100 days/stage CO₂ injection reaches a higher level than other case studies. The average pressure for 100 days/stage CO₂ injection is also higher than others, as shown in **Fig. 27(b)**.



(a) Bottomhole pressure

(b) Average reservoir pressure

Fig. 27 Effect of different CO₂ injection time on wellbore and reservoir pressure.

In this scenario, we notice that gas saturation in each case study has a huge difference, as shown in **Fig. 28**. With longer time of CO₂ injection, CO₂ can better diffuse into the reservoir which means higher depth and concentration. As the pressure is higher than MMP, CO₂ can dissolve into the oil. In turn, the oil with saturated CO₂ will swell, and expand. That is the primary mechanism to increase the reservoir pressure and lead to higher cumulative oil production.

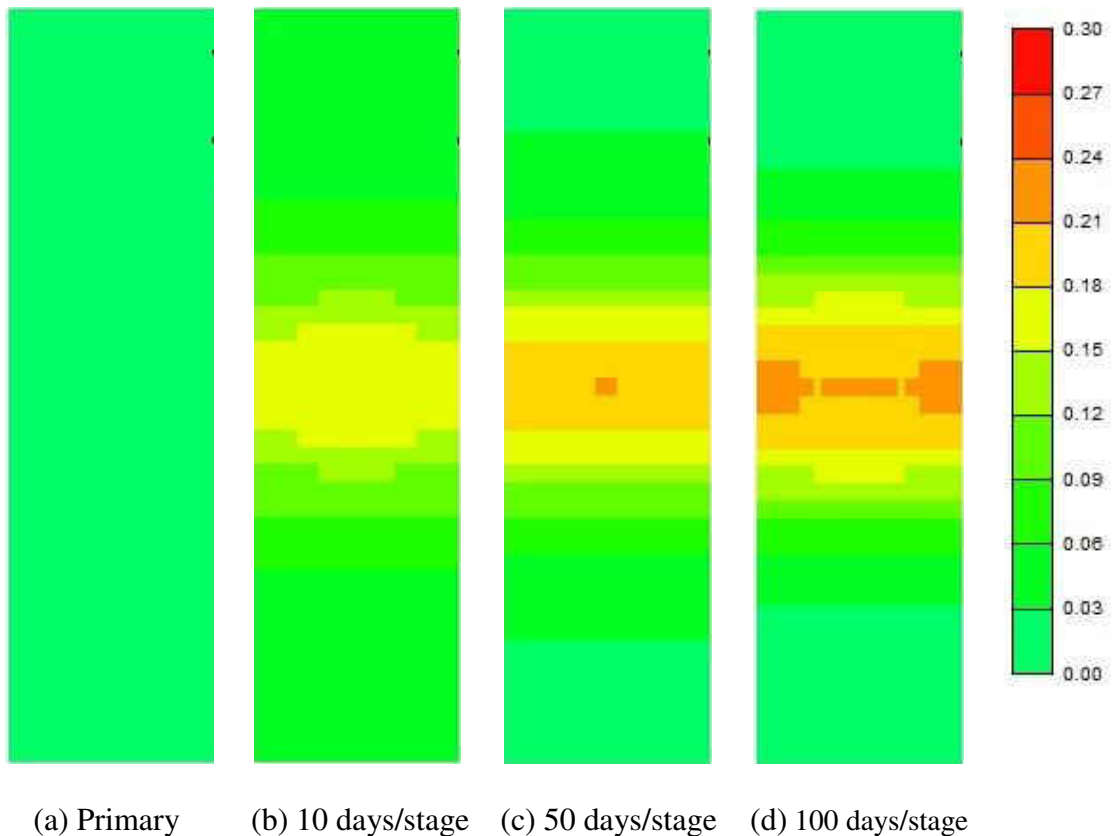


Fig. 28 Effect of different CO₂ injection time on reservoir CO₂ saturation.

Effect of CO₂ soaking time.

In this study, the CO₂ soaking time was adjusted from the base case, which is 14 days, to 7 days and 21 days to study the effect of different CO₂ soaking time for cumulative oil production. As shown in **Fig. 29**, the contribution to cumulative oil production after 7000

days is about 3.1%, 3.2% and 3.3% for the three CO₂ Huff-n-Puff cases with CO₂ soaking time of 7, 14 and 21 days, respectively.

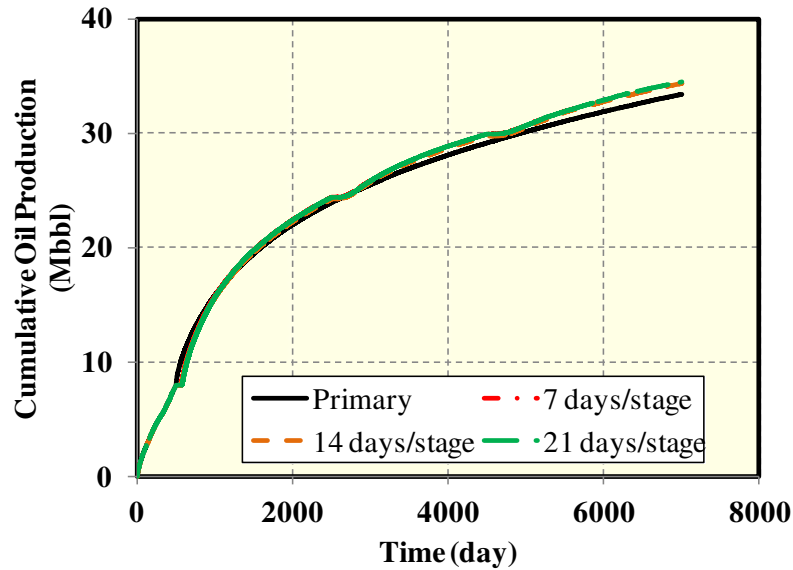
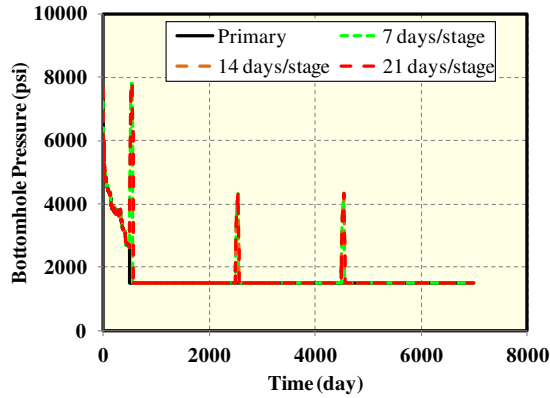
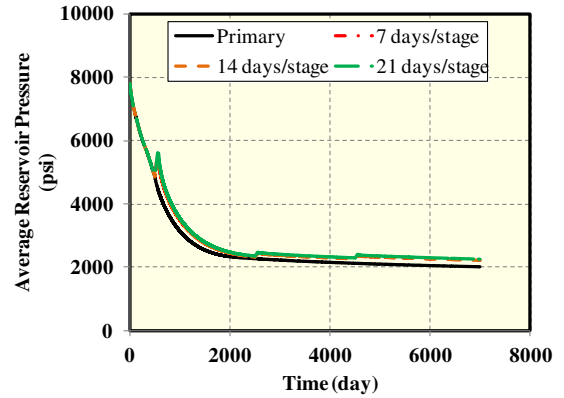


Fig. 29 Effect of different CO₂ soaking time on CO₂ Huff-n-Puff effectiveness.

Moreover, we compare the BHP and average reservoir pressure between these case studies, as shown in **Fig. 30**. Only a little difference can be found there. The various surfactant soaking time in this study yielded a small difference in cumulative oil production. The effect of soaking time may not be estimated accurately in the simulations because the mathematical models of multiphase flow generally assume a local thermodynamic equilibrium and disregards the reaction kinetics and the necessary interaction time for the surfactant to alter the rock wettability (Lotfollahi et al., 2017).



(a) Bottomhole pressure



(b) Average reservoir pressure

Fig. 30 Effect of different CO₂ soaking time on wellbore and reservoir pressure.

Effect of number of CO₂ Huff-n-Puff cycles.

Two more case studies were conducted to study the effect of number of CO₂ Huff-n-Puff cycles on oil recovery. 3 cycles, 1 cycle and 6 cycles of CO₂ Huff-n-Puff were studied in this scenario. The case study with only 1 cycle of CO₂ Huff-n-Puff process will start to inject CO₂ at 500th day. The other case with 6 cycles CO₂ Huff-n-puff process will start at 500th day, 1500th day, 2500th day, 3500th day, 4500th day and 5500th day, respectively. In each CO₂ Huff-n-Puff cycle, the well will be operated for 50 days CO₂ injection, and then shut in for 17 days of soaking. The remaining time will all be operated for production, with the constraint of minimum BHP which is 1500 psi. As shown in **Fig. 31**, after the history matching, the cumulative oil production of primary recovery become the highest one at first. At the time of 1300th day, the case with 1 cycle of CO₂ Huff-n-Puff cycle surpasses others and became the highest cumulative oil production, followed by 3 cycles and 6 cycles. At the time of 2200 day, the case with 6 cycles becomes the highest cumulative oil production, followed by 1 cycle and 3 cycles. And at the time of 5300th day,

the case with 3 cycles surpass the case with 1 cycles, but still lower than 6 cycles case. The contribution to cumulative oil production after 7000 days is about 1.6%, 3.2% and 4.6% for the three CO₂ Huff-n-Puff cases with cycles of 1, 3 and 6 times, respectively. All of the case studies with CO₂ Huff-n-Puff process have higher cumulative oil production than primary production. It indicates that CO₂ Huff-n-Puff is definitely beneficial for EOR. Also, with more CO₂ Huff-n-Puff cycles, cumulative oil production will be higher with long production time.

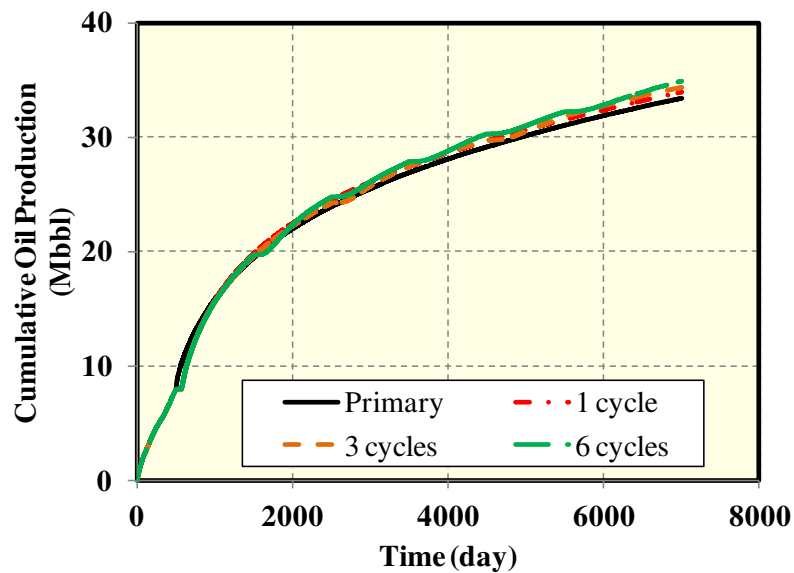


Fig. 31 Effect of different numbers of CO₂ Huff-n-Puff cycles on CO₂ Huff-n-Puff effectiveness.

With more CO₂ Huff-n-Puff cycles, the total volume of CO₂ injected increased, resulting in a higher oil production rate.

Effect of CO₂ molecular diffusion.

In this scenario, CO₂ molecular diffusion was studied. The range of CO₂ diffusion coefficient we considered was between 0.01 cm²/s to 0.001 cm²/s. More discussion about the range of molecular diffusion coefficient can be found by Yu et al. (2018). During the CO₂ Huff-n-Puff simulation, we only considered the CO₂ diffusion coefficient in both oil and gas phases. The diffusion coefficients of the other components were assumed to be zero.

The molecular diffusion coefficient in the base case was 0.005 cm²/s. In these two case studies, the CO₂ diffusion coefficient of 0.01 cm²/s and 0.001 cm²/s were assigned to each case. As shown in **Fig. 32**, the cumulative oil production indicates that with the higher CO₂ molecular diffusion coefficient leads to higher cumulative oil production. If the CO₂ molecular diffusion coefficient is extremely low, like the green line, which is 0.001 cm²/s, the CO₂ Huff-n-Puff leads to a lower oil production than the primary one. The contribution to the cumulative oil production after 7000 days is about 3.2% and 5.9% for the two cases with CO₂ diffusion coefficients of 0.005 and 0.01 cm²/s, respectively. For the case with CO₂ diffusion coefficients of 0.001 cm²/s, it decreased by about 1.3% compared to the primary production. Accordingly, the effect of CO₂ molecular diffusion is significant when evaluating the CO₂ Huff-n-Puff effectiveness in tight oil reservoirs. It is suggested that accurate measurements of CO₂ diffusion coefficients in the Middle Bakken oil reservoirs should be considered.

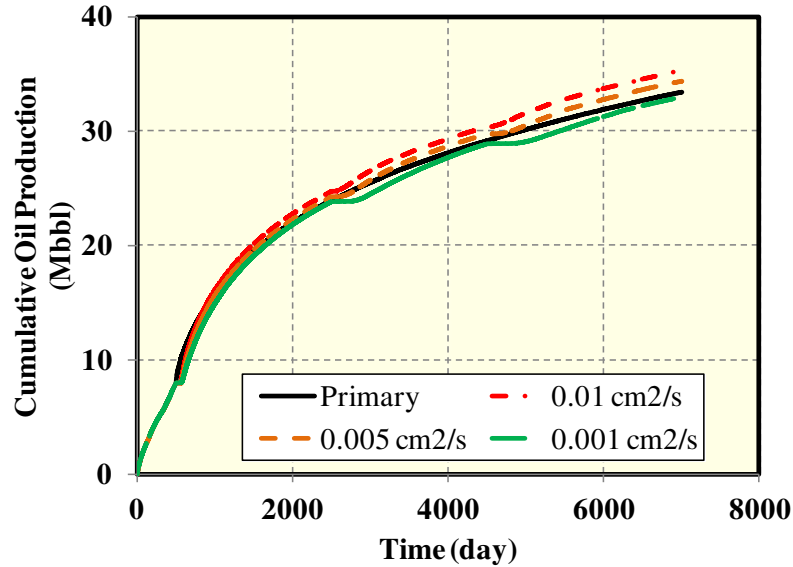


Fig. 32 Effect of different CO₂ molecular diffusions on CO₂ Huff-n-Puff effectiveness.

The effects of different CO₂ diffusion coefficients on cumulative CO₂ backflow are shown in **Fig. 33**. It clearly illustrates that more considerable amount of CO₂ will flow back to surface if the CO₂ diffusion coefficient is low. As a result, about 70% of CO₂ injected was produced back after 7000 days with the low CO₂ diffusion coefficient of 0.001 cm²/s, while 57% of CO₂ injected was produced back with the sizeable CO₂ diffusion coefficient of 0.05 cm²/s and 30% of CO₂ injected was produced back with the sizeable CO₂ diffusion coefficient of 0.01 cm²/s. The comparison of CO₂ gas mole fraction distribution after 7000 days CO₂ Huff-n-Puff between cases of 0 (primary), 0.001, 0.005 and 0.01 cm²/s is shown in **Fig. 34**. The CO₂ is 0 in the primary production case. However, it goes down with the CO₂ diffusion coefficient increase. As we mentioned before, with the same CO₂ injection, CO₂ flow back with the larger CO₂ coefficient is lower. It means that more CO₂ molecules can diffuse into the matrix porous with the larger CO₂ diffusion coefficient. So we can

believe that a better mixture of oil phase and CO₂ molecules results in higher cumulative oil production.

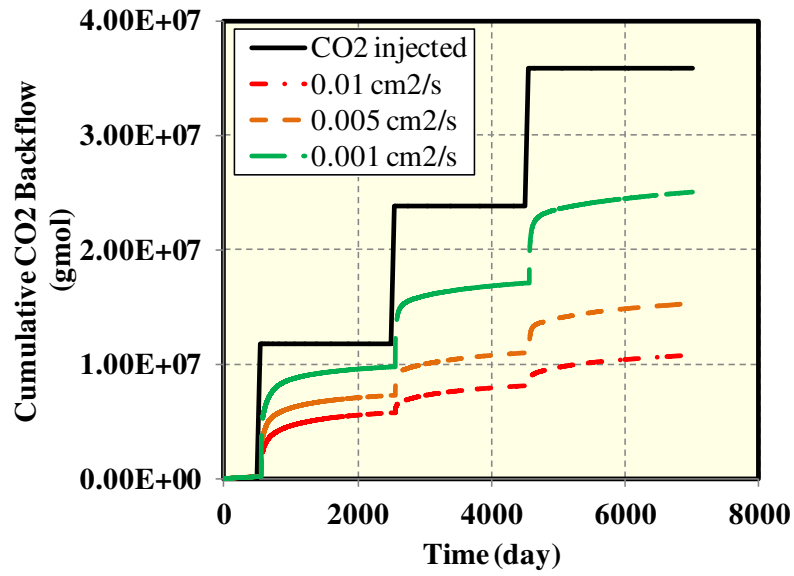


Fig. 33 Effect of different CO₂ molecular diffusions on the cumulative CO₂ backflow.

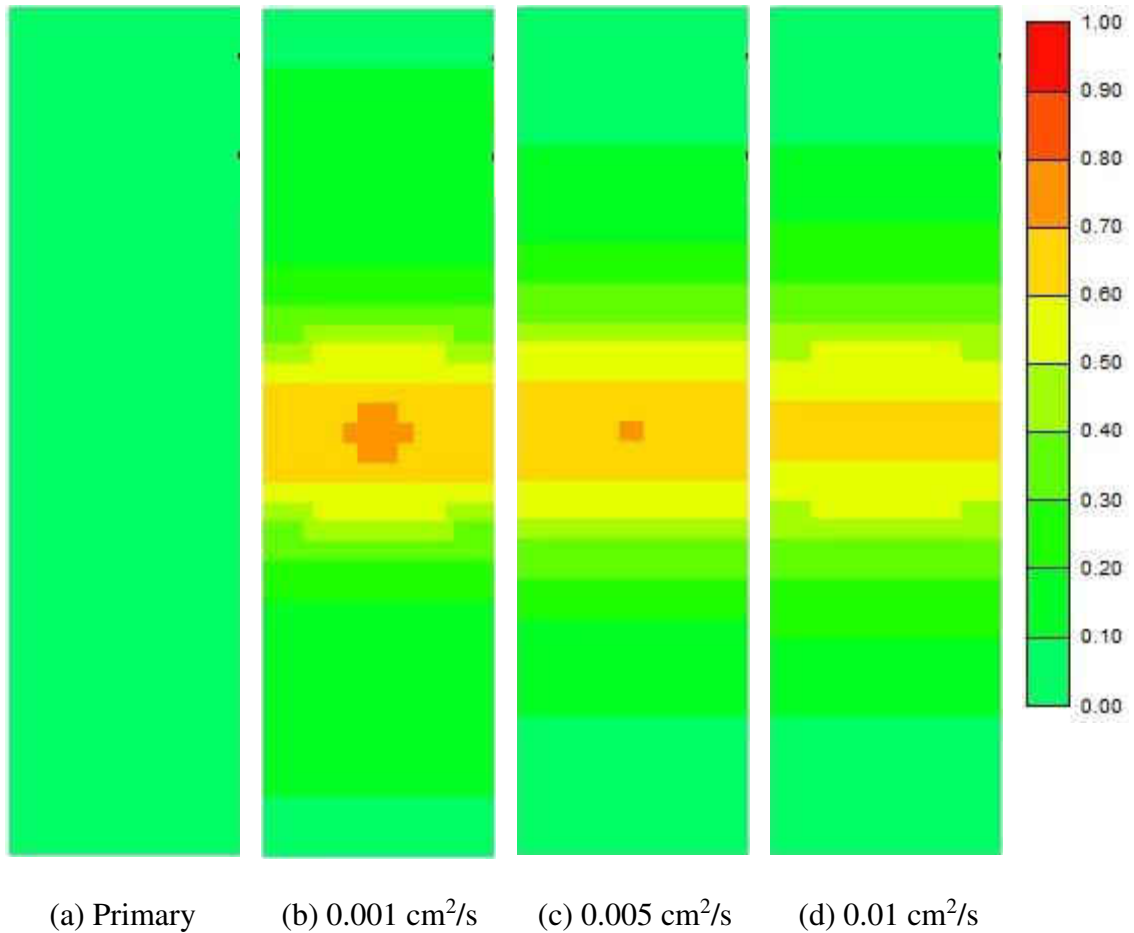


Fig. 34 Comparison of CO₂ gas mole fraction distribution after 7000 days CO₂ Huff-n-Puff.

In summary, the impacts of all uncertain parameters on the EOR effectiveness at 7000 days of production are shown in the Tornado plot (**Fig. 35**). It indicates that CO₂ diffusivity parameter has an extreme effect on EOR, followed by the number of CO₂ Huff-n-Puff cycle. CO₂ soaking time has only a slight effect on EOR, followed by CO₂ injection rate. The CO₂ injection time of each Huff-n-Puff cycle has a moderate effect on EOR. This ranking is based on the range of each parameter used in this study. The range for the incremental oil recovery factor at the time of 7000 days of production is about -1.3%–5.9%.

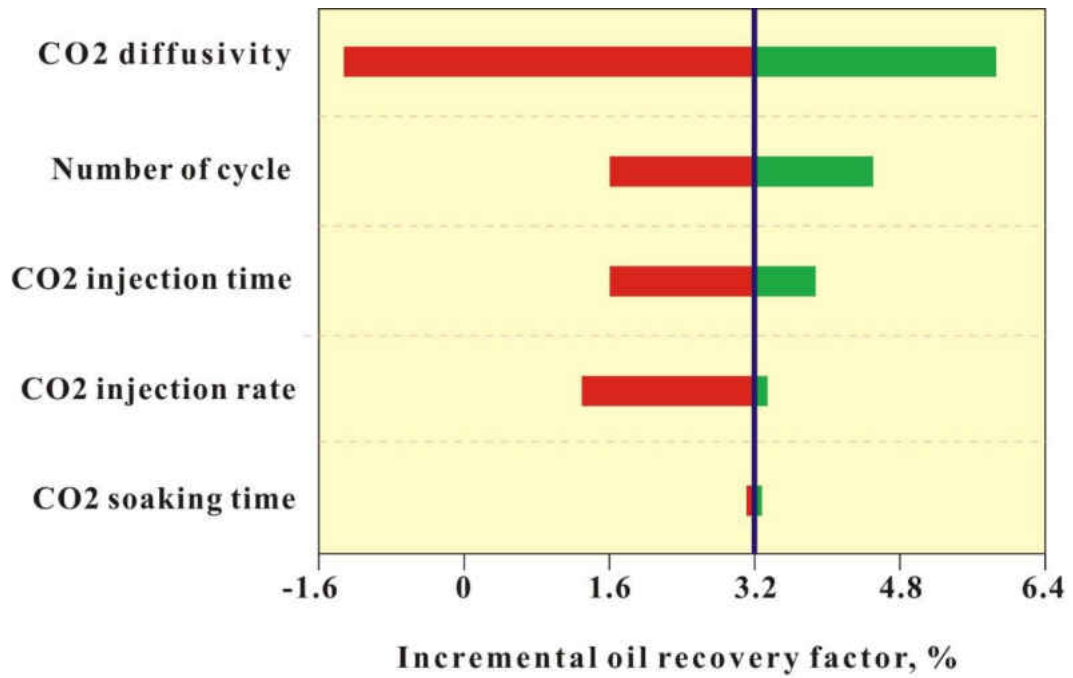


Fig. 35 Rank of impacts of five uncertain parameters on incremental oil recovery factor.

CHAPTER V

RESERVOIR SIMULATION OF FIELD SCALE SURFACTANT HUFF-N-PUFF PROCESS

5.1 Description of the Simulation Model

A homogeneous but anisotropic Middle Bakken simulation models was built up with the same reservoir property and hydraulic fractures according to one actual well. No flow boundary condition is assumed in these models. The specific data of the reservoir and hydraulic fractures are listed in **Table 6**.

Table 6. Field case reservoir model parameters.

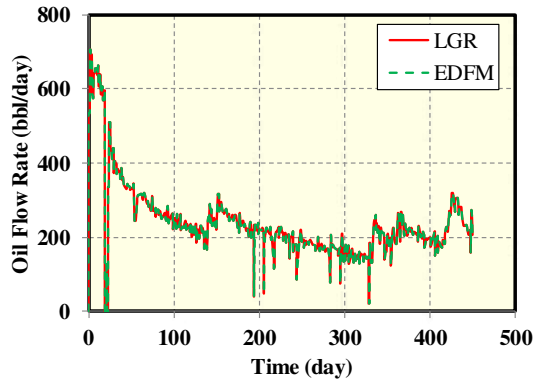
Parameter	Value	Unit
Model dimension (x×y×z)	10502×2640.2×50.4	ft
Number of gridblocks (x×y×z)	178×43×3	-
Initial reservoir pressure	7800	psi
Reservoir temperature	240	°F
Horizontal permeability	0.03	mD
Vertical permeability	0.003	mD
Reservoir porosity	5.6%	-
Initial water saturation	40%	-
Total compressibility	1×10^{-6}	psi ⁻¹
Reservoir thickness	50	ft
Well length	8555	ft
Number of stage	15	-
Clusters per stage	2	-
Cluster spacing	354	ft
Fracture half-length	92.1	ft
Fracture height	50.4	ft
Fracture width	0.01	ft
Fracture conductivity	500	md-ft

The Compositional data and Binary interaction parameters in this Middle Bakken well can be found in Chapter IV. The bubble point pressure of crude oil was 2501.253 psia, the oil API gravity was 42, the gas oil ratio was 853.04 scf/stb, the formation volume factor was 1.505, and the minimum miscible pressure (MMP) was 3260 psia. The water-oil relative permeability and liquid-gas relative permeability in this model were based on the literature (Yu et al., 2014b).

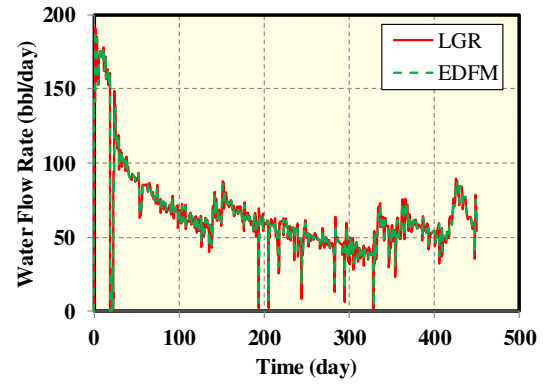
5.2 EDFM Validation

Base on the Middle Bakken simulation model in Chapter 4, a new Middle Bakken simulation model was built in EDFM. The difference is that one of these two models used an EDFM method to create the fracture grids. The other one used the LGR method to create the fracture grids, where each matrix grid containing fracture is set as $9 \times 1 \times 1$.

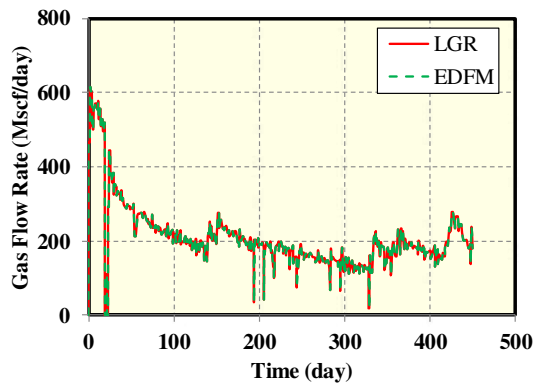
We operated the same production time with the same constraint conditions for these two models and compared the simulation results such as oil production rate, gas production rate, water production rate, and bottomhole pressure. An excellent agreement was achieved between EDFM and LGR, as shown in **Fig. 36**. Therefore, we can deem the accuracy of the EDFM method that is the same as LGR method in reservoir simulation model on the basis of our validation results. We can use the EDFM method to do our production prediction study.



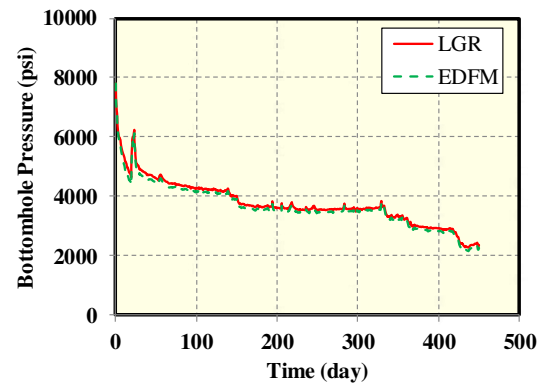
(a) Oil flow rate



(b) Water flow rate



(c) Gas flow rate



(d) Bottomhole pressure

Fig. 36 Comparison of well performance and BHP between LGR and EDFM.

Moreover, we found that the EDFM method provides more significant computational efficiency than the LGR method. There is a considerable difference between the LGR and the EDFM methods, which is the CPU time needed for simulation running. The LGR method used 3909 seconds to run the case. However, the EDFM method only use 2650 seconds to run the same case. The EDFM method saved about 30% simulation running time compared with the LGR method. In this case, we used the EDFM method to continue our following simulation case studies.

5.3 History Match in Field Case

The history match of an actual well with 451 days of available production data from Middle Bakken is placed in this section (Kurtoglu and Kazemi, 2012).

A field-scale reservoir model was developed to use the commercial simulator CMG-STARs in combination with EDFM software to simulate a surfactant flooding experiment. Thirty bi-wing hydraulic fractures were inserted into the model, and a horizontal well penetrated the middle of all the fractures. The model dimension is 10502 ft × 2640.2 ft × 50.4 ft, which corresponds to the length, width, and height, respectively, as shown in **Fig. 37**.

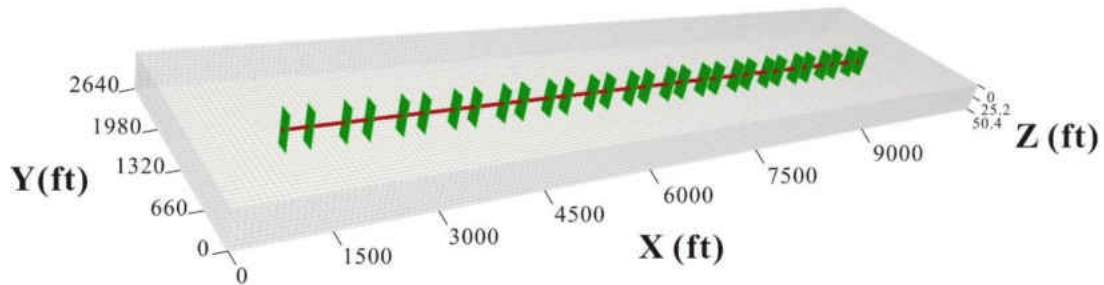


Fig. 37 A field-scale reservoir model with a horizontal well and 30 bi-wing hydraulic fractures.

In our history matching simulation, the oil rate measured from the field is used as a constraint input, as shown in **Fig. 38**. Gas rate and bottomhole pressure (BHP) are the targets for history matching. Fracture half-length, fracture conductivity, and matrix permeability were mainly used as the tuning parameters to achieve good match results.

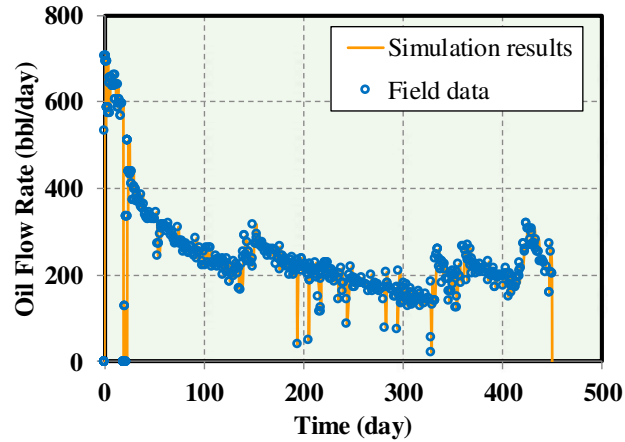
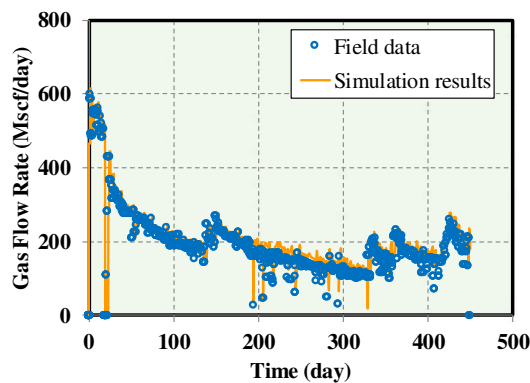
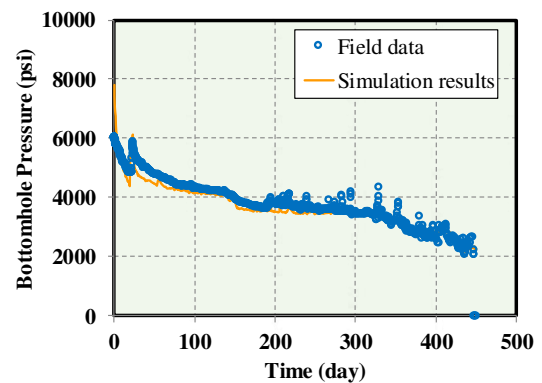


Fig. 38 Oil flow rate comparison between actual Middle Bakken well data and model results.

As shown in **Fig. 39(a)** and **Fig. 39(b)**, a great match between the simulation results and actual field production data were achieved for gas rate and bottomhole pressure, respectively. Moreover, based on the excellent history match, we found that the fracture conductivity is 500 md-ft, fracture half-length is 92.1 ft, and matrix permeability is 0.02 md.



(a) Gas flow rate



(b) Bottomhole pressure

Fig. 39 Comparison of gas flow rate and bottomhole pressure between real well production data and simulation model results.

5.4 History Match in Section Model

A section model, which has only one stimulation stage (two bi-wing hydraulic fractures), was built up as shown in **Fig. 40**, in order to overcome the computational burden.

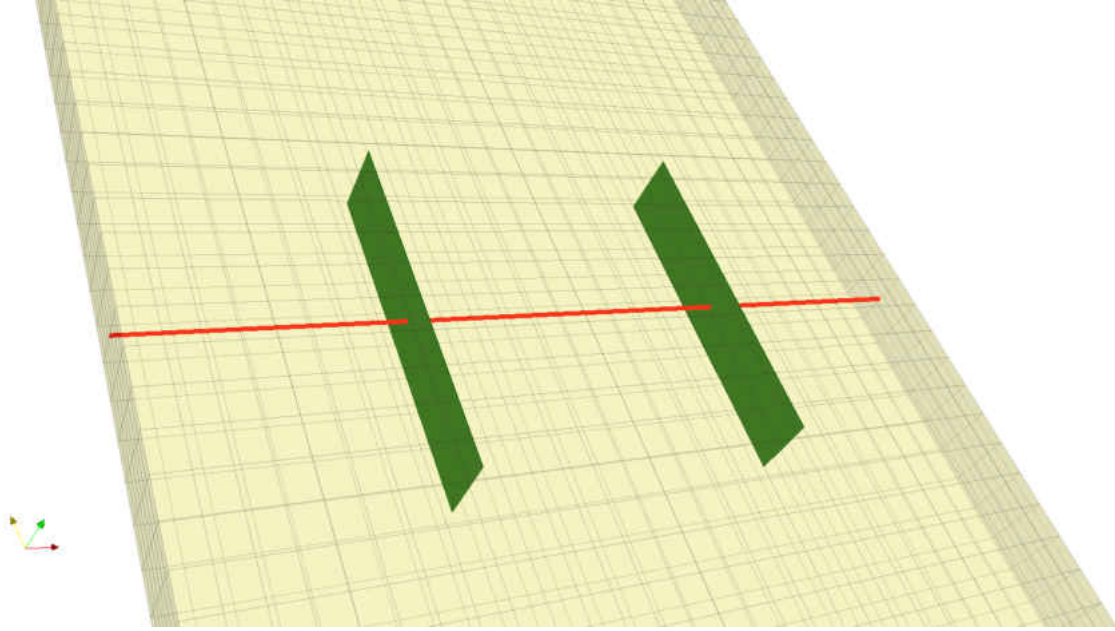


Fig. 40 A section model with a horizontal well and two bi-wing hydraulic fractures.

We also ran the grid sensitivity analysis with different grid sizes in the Z direction. For instance, on account of the used forward-difference approximation to the truncation Darcy flow equation (Explicate formulation), and the capacity of our computer is not able to carry an infinite number of digits, the solution would differ from the exact solution of the original partial differential equation (PDE). Therefore, the Truncation-Error Analysis needs to be placed before the prediction of sensitivity study:

$$e_L = \left[\frac{(\Delta x)^2}{12} \frac{\partial^4 p}{\partial x^4} \Big|_i^n - \frac{(\Delta t)}{2D_i} \frac{\partial^2 p}{\partial x^2} \Big|_i^n \right] \quad (9)$$

or

$$e_L = O[(\Delta x)^2] + O(\Delta t) \quad (10)$$

where e_L is the truncation error, Δx is the grid size and Δt is the time step.

It was found that the smaller Δx is, the smaller truncation error can achieve (Turgay et al., 2001). The same results can be got from the backward-difference approximation and central-difference approximation.

In this grid sensitivity analysis, we injected two cycles of 0.2% surfactant in 1000STB/day, with 300 days injection and 20 days soaking after the history match period. The surfactant adsorption parameter is 1 lbmole/ft³. As we mentioned before, the equation of Truncation-Error indicates that the smaller grid size will have less Truncation-Error. The assumption is that the simulation will be more accurate with the decrease of grid size. Therefore, according to the simulation results shown in **Fig. 41**, the section model with 7, 9 and 11 layers in the Z direction are relatively accurate.

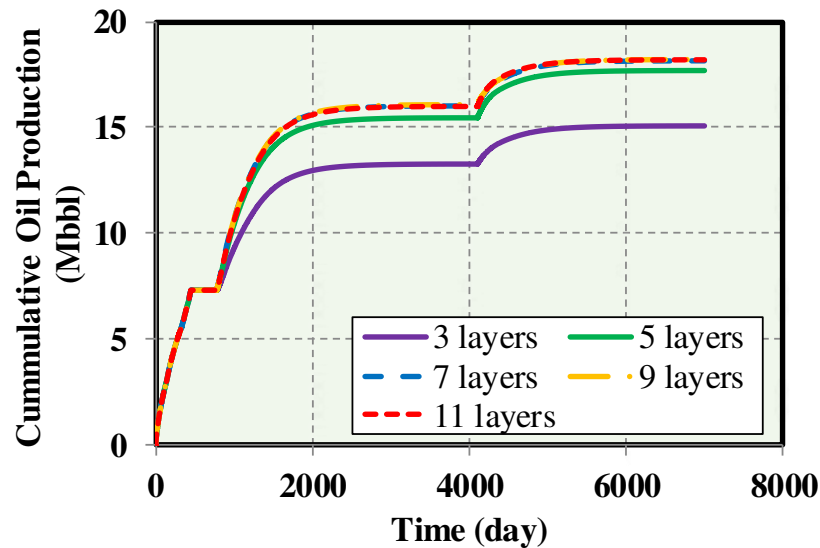


Fig. 41 Cumulative oil production comparison between different grid layers with surfactant flooding case.

Although the accuracy of these three cases is all relatively accurate, the CPU seconds for them have huge differences, which are 4888, 9138 and 10787 seconds. Seven layers model was selected as the optimal one considering the accuracy and CPU time to continue our section model history match. The detailed input parameters for our model are listed in

Table 7. All the reservoir characterizations are similar to the field case, for example, the fracture conductivity, fracture half-length, and so on.

Table 7. Section model parameters.

Parameter	Value	Unit
Model dimension (x×y×z)	580×2150×50.4	ft
Number of gridblocks (x×y×z)	30×86×7	-
Initial reservoir pressure	7800	psi
Reservoir temperature	240	°F
Horizontal permeability	0.03	mD
Vertical permeability	0.003	mD
Initial water saturation	40%	-
Total compressibility	1×10^{-6}	psi ⁻¹
Reservoir thickness	50.4	ft
Well length	578.8	ft
Stage spacing	236	ft
Fracture half-length	92.1	ft
Fracture height	50.4	ft
Fracture width	0.01	ft
Fracture conductivity	500	md-ft

The oil rates from the actual well production data were set as the well constraint. Because the fractures and field dimensions are 15 times smaller than the actual field model, the actual well performance was divided by 15, as shown in **Fig. 42**.

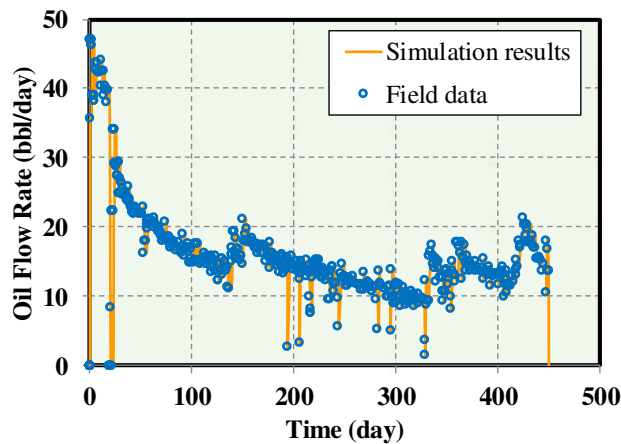


Fig. 42 Oil flow rate comparison between actual well data and section model results.

Comparing the gas flow rate and bottomhole pressure, there is also a great history match achieved in this model, as shown in **Fig. 43**. It proves that the section model can be used to continue our surfactant flooding studies.

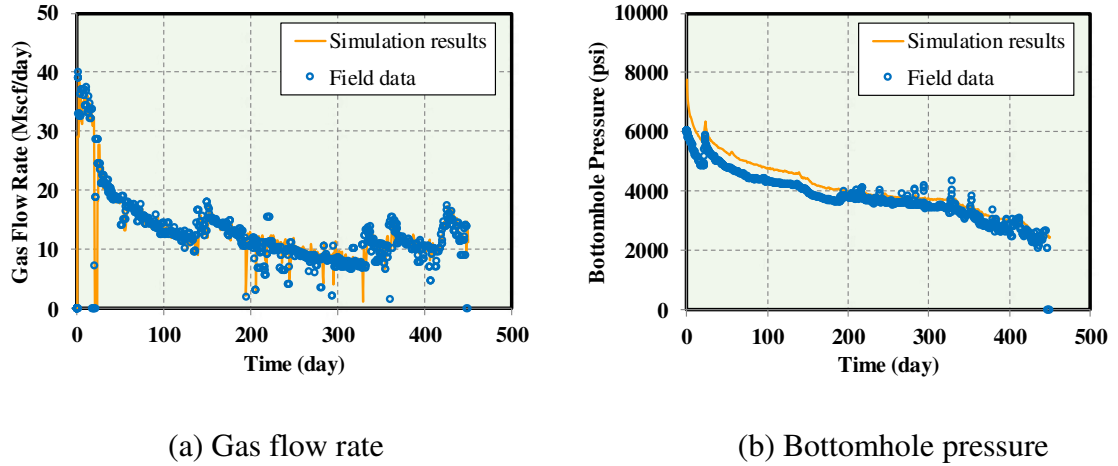


Fig. 43 Comparison of gas flow rate and bottomhole pressure between modified well production data and simulation model results.

5.5 Wettability Alteration

Wettability alteration in this model depends on the adsorbed surfactant concentration. It is based on a scaling factor averaged linear interpolation scheme. Since the surfactant isotherm may reach a plateau at some critical surfactant concentration, which is called the Critical Micelle Concentration (CMC), and the injected surfactant concentration is normally much higher than the CMC, Langmuir-type isotherm is applied to the adsorption process (Stars Menu):

$$ad = \frac{(tad1+tad2 \times xnacl) \times ca}{(1+tad3 \times ca)} \quad (11)$$

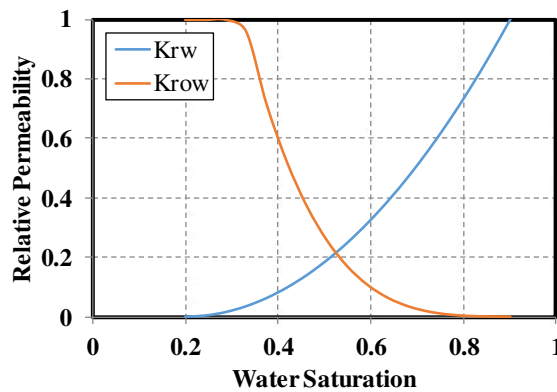
where ad is the adsorbed moles per unit pore volume, $xnacl$ is the salinity of the brine, ca is the mole fraction of surfactant in the oil phase, $tad1$ is the adsorption parameter, $tad2$ is the adsorption isotherm associated with salt effects, and $tad3$ is the parameter coefficient.

Since the wettability alteration depends on the level of surfactant adsorption, the Wettability Alteration Parameter (ω) is used to represent the amount of surfactant adsorbed onto the rock surface (Delshad et al., 1996):

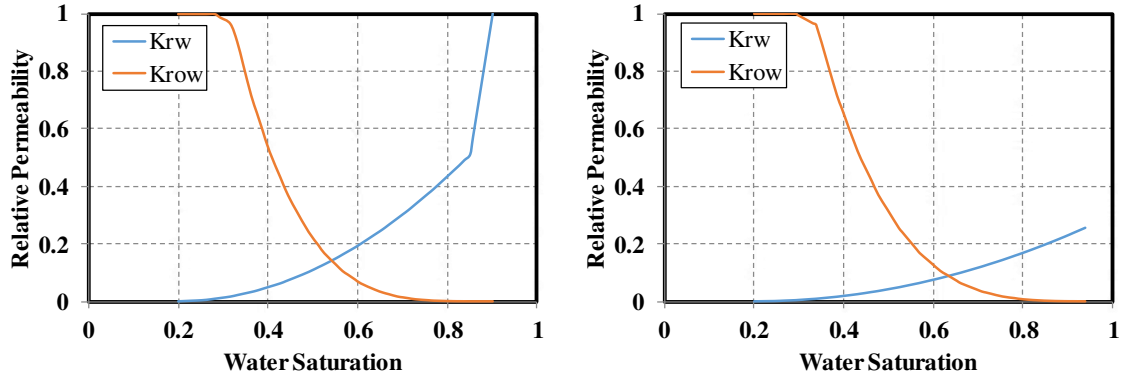
$$\omega = \frac{\hat{C}_n}{C_n + \hat{C}_n} \quad (12)$$

where C_n is the total concentration of nanofluids and \hat{C}_n is adsorbed concentration of nanofluids.

Wettability is an important parameter that will influence the EOR. It will not increase the oil production directly but affect the fluid saturation and their distribution in the porous media. In this study, we used the modification of relative permeability and capillary pressure curves to represent the wettability alteration in commercial simulation software (CMG-STAR3). The rock wettability is gradually altered from oil-wet to water-wet. We inputted three different rock types which are oil-wet, mixed-wet and water-wet as shown in **Fig. 44**. Then we used the simulator to interpolate them and get complex dynamic relative permeability curves along with the surfactant adsorbed into the reservoir. So did the capillary pressure. The capillary pressure data in the model were based on the literature (Masalmeh., 2002; Anderson., 2006), as shown in **Fig. 45**.



(a) Oil-wet ($\omega=0$)



(b) Mixed-wet ($\omega=0.5$)

(c) Water-wet ($\omega=1$)

Fig. 44 Three inputted oil-water relative permeability curves for different rock wettability conditions.

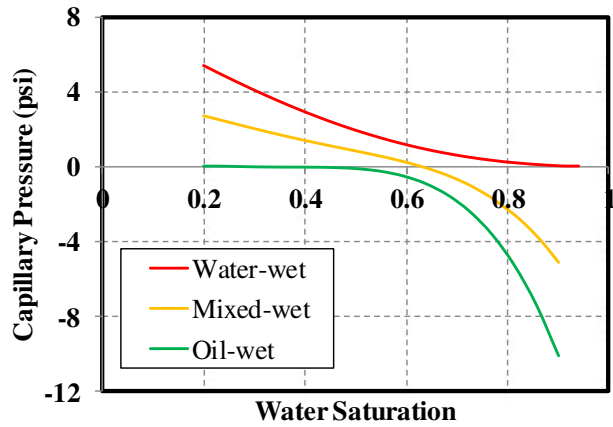


Fig. 45 Three inputted capillary pressure curves for different rock wettability conditions (Masalmeh., 2002; Anderson., 2006).

The IFT data were selected from the literature (Yang, 2018), as shown in **Table 8**. We used the Langmuir isotherm coefficients to define the surfactant adsorption, so the surfactant adsorption depends on the surfactant concentration in the microemulsion, as shown in **Fig. 46**.

Table 8. Surfactant IFT table.

Surfactant Concentration	Interfacial Tension (dyn/cm)
0	23.1
0.1	0.17
0.2	0.014
0.3	0.0047
0.4	0.0089
0.5	0.0154

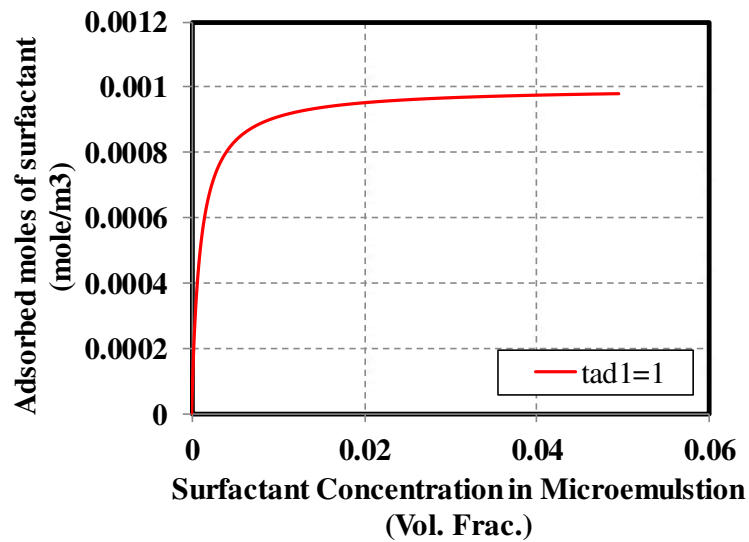


Fig. 46 The Langmuir adsorption isotherm curve.

5.6 Surfactant Effectiveness Verification

As an uncertainty chemical fluid we simulated, the first thing we supposed to do is to verify the effectiveness of this surfactant. We compared this surfactant flooding in Huff-n-Puff case with the primary production, as shown in **Table 9**. In the primary production case, the production well was producing the oil with a constraint that the minimum BHP was 1500 psi after the history match period. For the surfactant Huff-n-Puff case, there were two cycles of Huff-n-Puff set as the well constraints. In each Huff-n-Puff case, the injection well injected the water with 0.2% surfactant for 300 days at the rate of 1000 bbl/day and constrained the maximum BHP to 7800 psi. The injection well was shut in for 20 days soaking after that. It is one cycle of the surfactant Huff-n-Puff, the production well also used the constrained with minimum BHP of 1500 psi.

Table 9. Time steps comparison between surfactant flooding and primary production.

Time (days)	Primary production	Surfactant flooding
0	History match	History match
450	Produce	Surfactant injection
750	Produce	Soaking
770	Produce	Produce
3775	Produce	Surfactant injection
4005	Produce	Soaking
4025	Produce	Produce
7000	STOP	STOP

The comparison of simulation results for cumulative oil production is shown in **Fig. 47**. After the second Huff-n-Puff cycle, the oil recovery factor achieves a much higher value than the primary production, about 0.9% oil recovery factor increase. Therefore, the surfactant flooding is more efficient than the primary production.

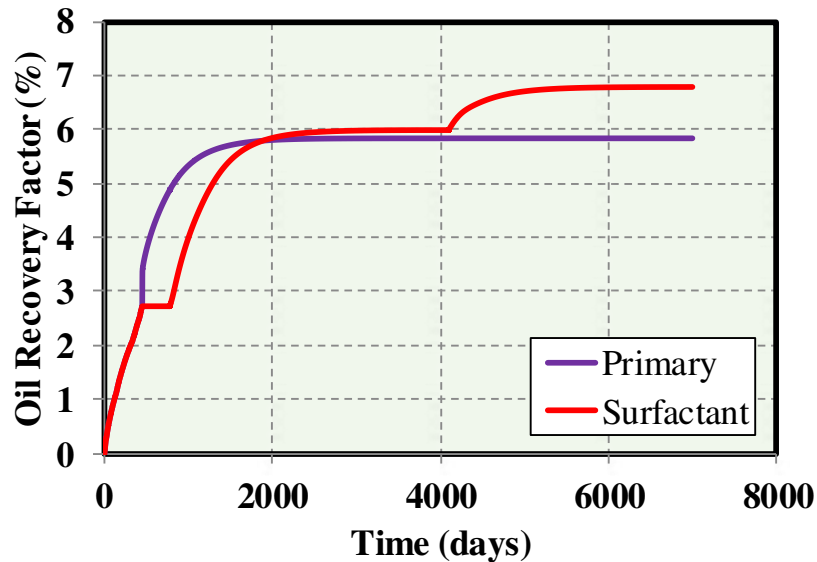
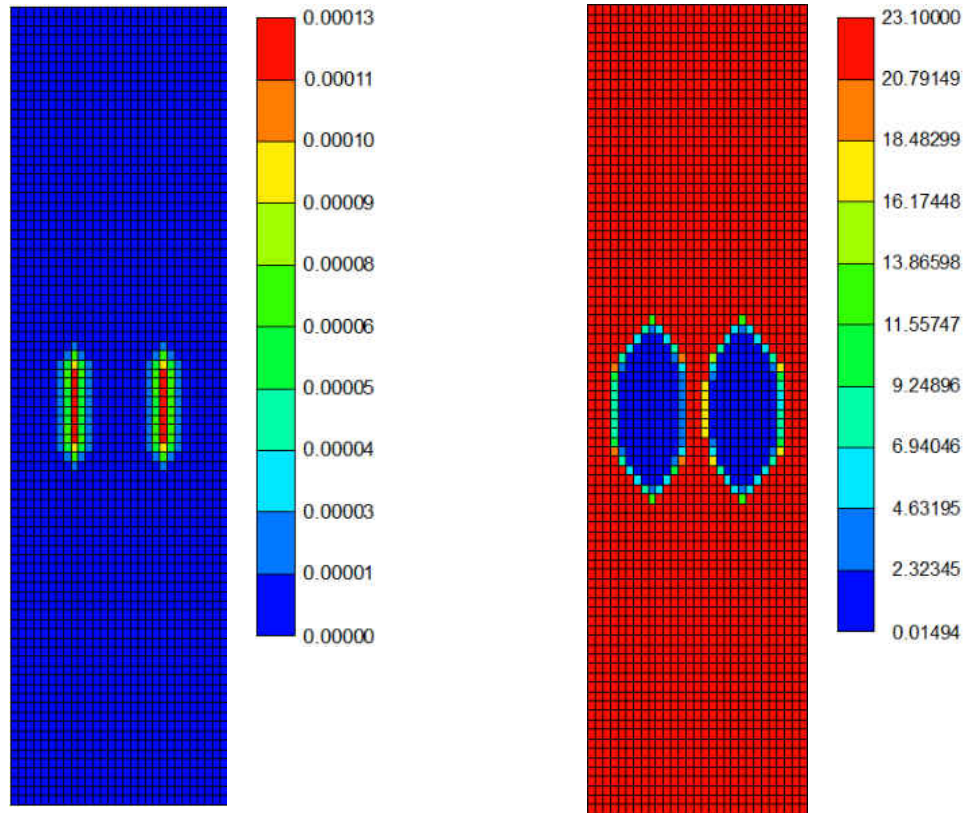


Fig. 47 Oil recovery factor comparison between the primary production and surfactant flooding case.

We consider the reason for this increased oil recovery factor is the effect of surfactant. To discover the effect of surfactant, the adsorbed surfactant map is shown in **Fig. 48 (a)**, and the IFT map is shown in **Fig. 48 (b)**. For the grids close to the fracture, higher surfactant concentration appeared to comparing with the grids far from the fractures. It denotes that

the IFT reduced with the surfactant adsorbed into the rock. With the lower IFT, and the rock wettability changed from oil-wet to water-wet, the oil production increased. Therefore, we can verify that the surfactant flooding is able to increase oil recovery due to the wettability alteration.



(a) Adsorbed Surfactant (lbmole/ft³) (b) Interfacial tension (dyne/cm)
Fig. 48 Adsorbed mole of surfactant and IFT in the end of surfactant flooding.

5.7 Sensitivity Analysis

In order to discover the Huff-n-Puff effects on surfactant EOR in the Middle Bakken, six scenarios were designed in this section. All the parameters studied here are in reasonable ranges, and only one parameter is modified in each scenario. The parameters are surfactant adsorption, surfactant injection time, soaking time, surfactant injection rate, surfactant concentration and the number of surfactant Huff-n-Puff cycles.

The maximum BHP was set to be 7800 psi, based on the initial reservoir pressure. The minimum BHP was set as 1500 psi, which according to the literature review. **Table 10.** summarizes the value of parameters we used for sensitivity studies.

Table 10. Parameters and their range for surfactant Huff-n-Puff sensitivity analysis.

	Low	Base	High
Adsorption (lbmole/ft ³)	0.5	1	1.5
Days of injection	150	300	450
Days of soaking	5	20	35
Number of cycles	1	2	3
Injection rate (STB/day)	500	1000	1500
Surfactant concentration	0.0005	0.002	0.005

Effect of Surfactant Adsorption

In this scenario, the surfactant adsorption parameter (tad) was changed from 1 lbmole/ft³ to 0.5 lbmole/ft³ and 1.5 lbmole/ft³, the surfactant adsorption curves are shown in **Fig. 49.**

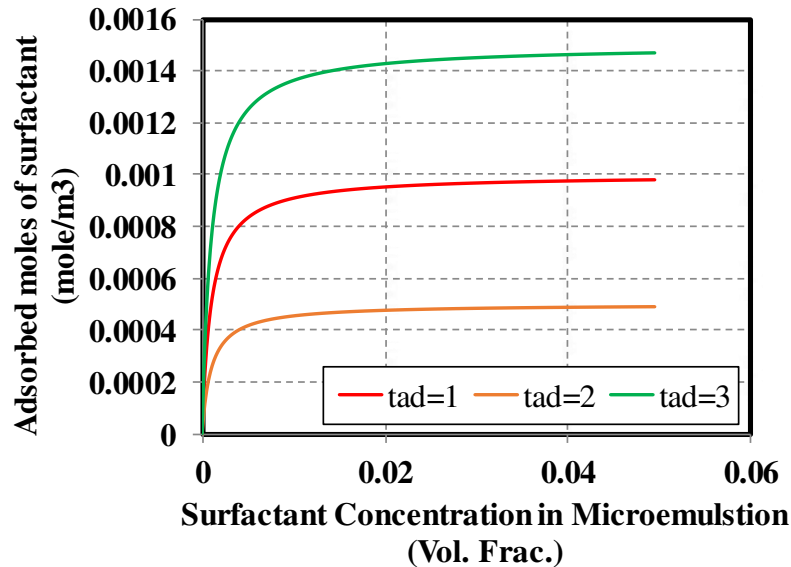


Fig. 49 The comparison of three different Langmuir adsorption isotherm curves.

Other parameters were kept as usual. These three case studies were compared with the base case and primary production. As shown in **Fig. 50**, after the history matching period, the cumulative oil production without Surfactant injection (primary production) is the highest

one, followed by 0.5 lbmole/ft³, 1.0 lbmole/ft³ and 1.5 lbmole/ft³ in sequence. At the time of 1700 days which is the middle of the first CO₂ Huff-n-Puff cycle, the cumulative oil productions are closed to each other and almost at the same level. After 1700 days, the case with high surfactant adsorption becomes the highest cumulative production oil case, followed by other lower surfactant adsorption in sequence. At the end of the simulation, the cumulative oil production with the 1.0 lbmole/ft³ surfactant adsorption is close to the case with 0.5 lbmole/ft³ surfactant adsorption, but comparably much lower than the case with 1.5 lbmole/ft³ surfactant adsorption. The contribution to cumulative oil production after 7000 days is about 14.4%, 16.4% and 20.0% for the three surfactant Huff-n-Puff cases with the surfactant adsorption of 0.5 lbmole/ft³, 1.0 lbmole/ft³ and 1.5 lbmole/ft³, respectively. The higher adsorption leads to a higher cumulative oil production, which indicates that the high surfactant adsorption is beneficial for EOR without considering the economic benefits.

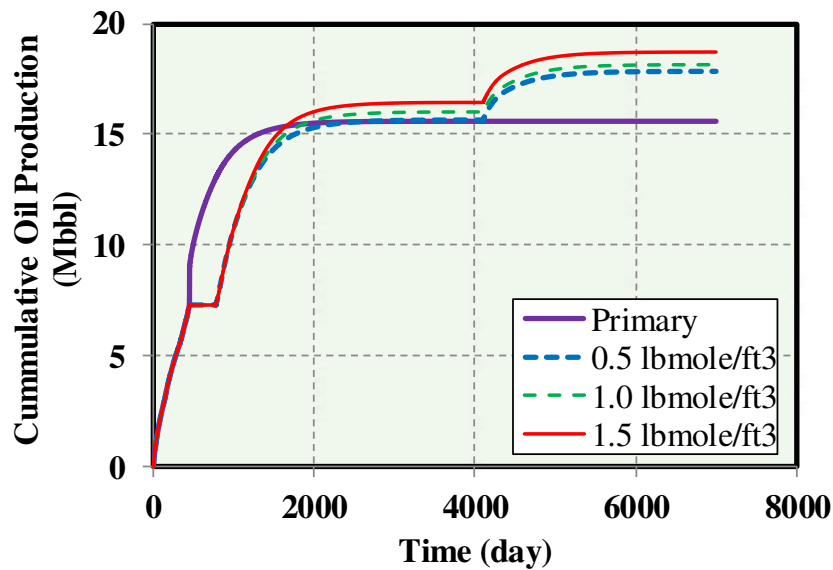


Fig. 50 Effect of different surfactant adsorption on surfactant Huff-n-Puff effectiveness.

Effect of Surfactant Injection Time.

According to the base case, two more case studies conducted in this surfactant injection time scenario. The surfactant injection time was modified from the base case, which was 300 days/stage, to 150 days/stage and 450 days/stage. Other parameters were not changed. The base case and primary production were also used as the reference to compare the incremental oil production. As shown in **Fig. 51**, after the history match period, the primary production is the highest one. At the time of 1500 days, the case with 150 days/stage injection time surpassed the primary production and became the highest oil production. At the time of 1800 days, the base case which is 300 days/stage injection time became the highest one. The case with 450 days/stage injection time is still the lowest production until the time at 2200 days. However, this case has the highest oil production at the end of the simulation which is 18.3% higher than primary production. The case with 150 days/stage and 450 days/stage were 15.5% and 16.4% higher than the primary production, respectively. According to the simulation results with different injection time, the surfactant Huff-n-Puff process with longer injection time has higher oil recovery in the end. Moreover, because the case with higher injection time had less oil recovery in the beginning, we regard this incremental oil recovery as the potential oil recovery. So, it is crucial to design an optimum ratio between injection time and production time according to the total working time of the well.

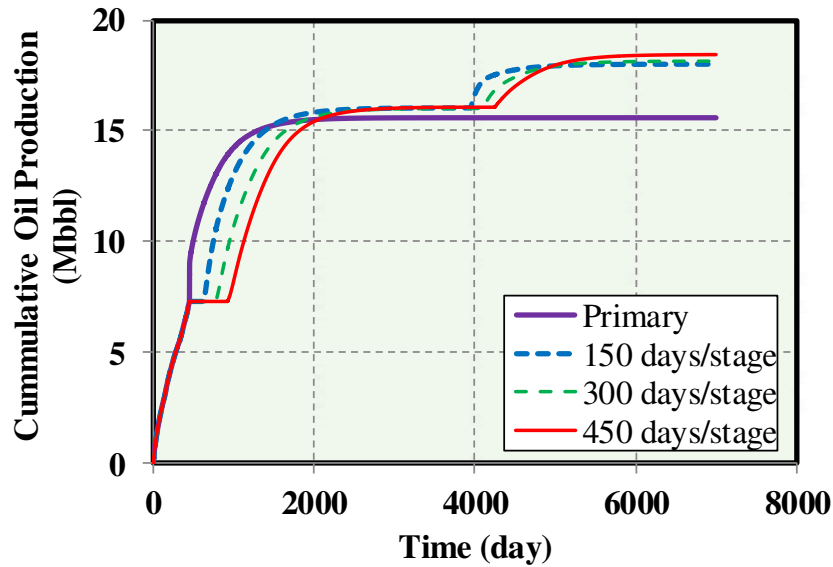


Fig. 51 Effect of different CO₂ injection times on CO₂ Huff-n-Puff effectiveness.

Effect of Surfactant Soaking Time.

In this surfactant soaking time scenario, there were also two more case studies conducted. The surfactant soaking time was modified from 20 days/stage to 5 days/stage and 35 days/stage. After the history match period, the case with 35 days/stage soaking time surpassed the primary production at first, at the time of 1700 days, as shown in **Fig. 52**. Then this curve kept lead the cumulative oil production until the end of the simulation, and the incremental oil production reached 19.0%. The case with 20 days/stage which is the base case and the case with 5 days/stage all behind this case. The cumulative oil production for these two cases is 16.4% and 16.0%, respectively. The difference in surfactant soaking time in this study showed a little difference in cumulative oil production.

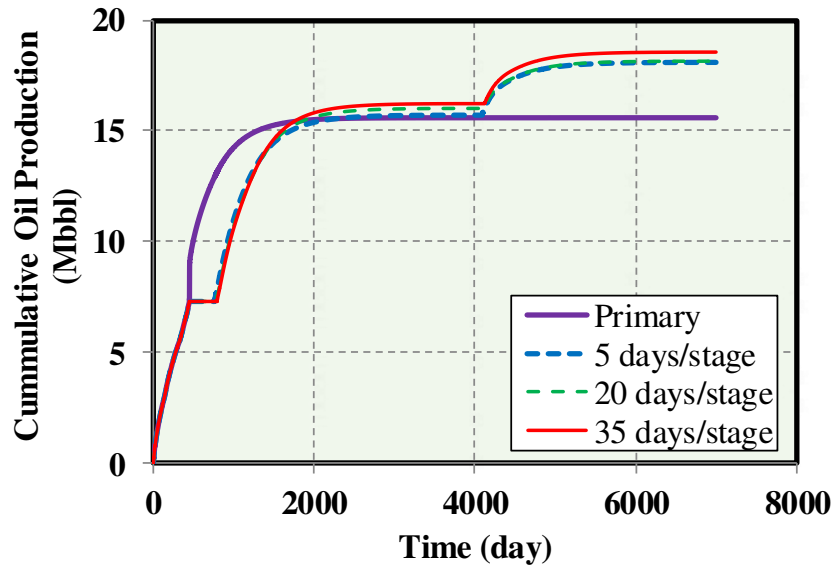


Fig. 52 Effect of different CO₂ soaking times on CO₂ Huff-n-Puff effectiveness.

Effect of time on Surfactant Huff-n-Puff Cycles.

Two more case studies were conducted for the surfactant Huff-n-Puff cycles scenario. The time of the surfactant Huff-n-Puff cycles was changed from the base case, which has 3 cycles, to 1 cycle and 6 cycles. The case study with 1 cycle of surfactant Huff-n-Puff process started at the time of 450 days. The case 2 has one more cycle which started at the time of 3775 days. Also, a case with 3 cycles started at the time of 450 days, 2650 days and 4800 days. As shown in **Fig. 53**, after the history match period, the primary production had the highest cumulative oil production. After the first Huff-n-Puff cycle, all three cases surpassed the primary production. Higher oil production attained with more Huff-n-Puff case conducted according to three cases. The incremental oil production for these one, two and three cycles were 2.7%, 16.4% and 25.2%, respectively. All of the cases with the Huff-n-Puff process have higher cumulative oil production than the primary production. Therefore, the surfactant Huff-n-Puff process is beneficial for EOR. The incremental oil production will increase while the number of Huff-n-Puff cycles increase. However, as we

can see, with the Huff-n-Puff cycles increase, the degree of incremental oil production is decreasing. It means that with more surfactant Huff-n-Puff cycles, like 5 or 6 cycles, the incremental oil production may not increase a lot. However, we can still have the conclusion that with more surfactant Huff-n-Puff cycles, the higher cumulative oil production we will get.

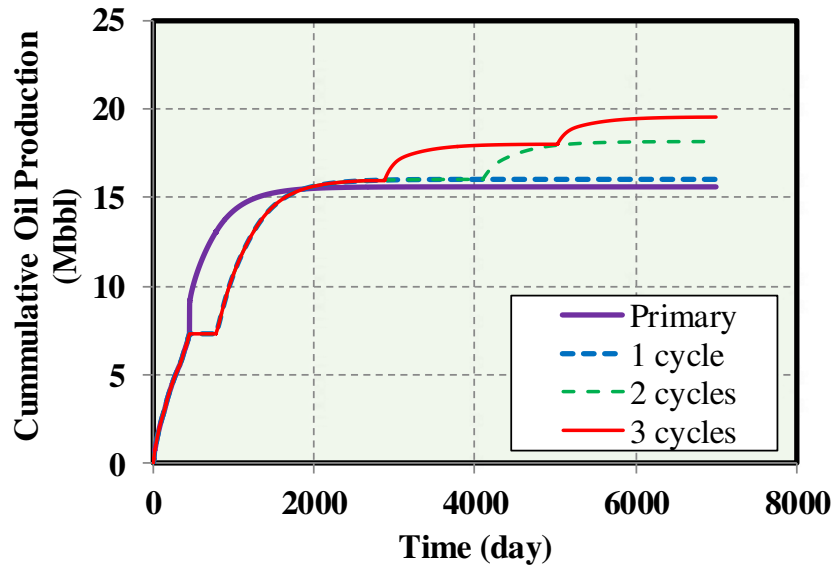


Fig. 53 Effect of different numbers of CO₂ Huff-n-Puff cycles on CO₂ Huff-n-Puff effectiveness.

Effect of Surfactant Injection Rate.

In this surfactant injection rate scenario, we discovered the relationship between the different surfactant rates and cumulative oil production. The surfactant injection rates were considered to be 500 bbl/day, 1000 bbl/day and 1500 bbl/day. As shown in **Fig. 54**, three case studies all surpassed the primary production at the time of 2000 days. Also, they have almost the same cumulative oil production at the end of the simulation. The incremental oil production for these three cases were 16.7%, 16.4% and 14.7%, respectively. Under the condition of limiting the maximum bottomhole pressure, the results of three case studies

with different surfactant injection rates do not have a significant difference. So, if the surfactant injection rate is high enough to reach the maximum bottomhole pressure within a short period, the effect of increasing the injection rate is not significant.

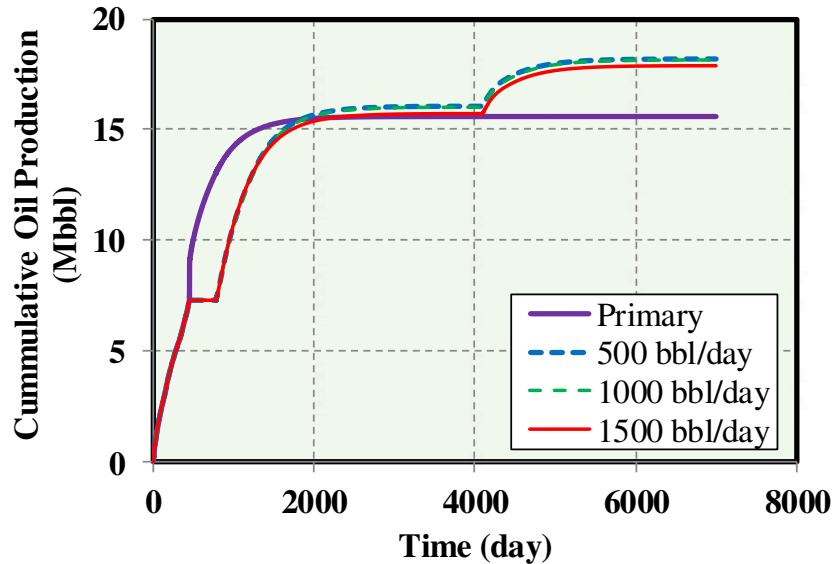


Fig. 54 Effect of different surfactant injection rate on CO₂ Huff-n-Puff effectiveness.

Effect of Surfactant Concentration.

In this surfactant concentration scenario, there were two more case studies conducted. The range of surfactant concentration varied from 0.05% to 0.5% that would be able to have an economic benefit. As shown in **Fig. 55**, the surfactant concentration of 0.5 % (red line) keeps leading the highest cumulative oil production during the whole simulation time comparing with the other two case studies. Moreover, this high surfactant concentration line is also the first line which surpasses the primary production. Compared with other sensitivity studies, it is not difficult to find that the concentration of the surfactant can increase the oil production directly and do not have any hesitate time, like the surfactant injection time, soaking time, Huff-n-Puff cycles, and so on. The incremental oil production of the surfactant concentration with 0.05%, 0.2% and 0.5% are 1.1%, 16.4% and 19.4%,

respectively. It indicates that with the higher surfactant concentration, the cumulative oil production should be higher. However, the surfactant cost is high, it also suggested that the proper balance between the surfactant concentration and incremental oil production needed to be considered.

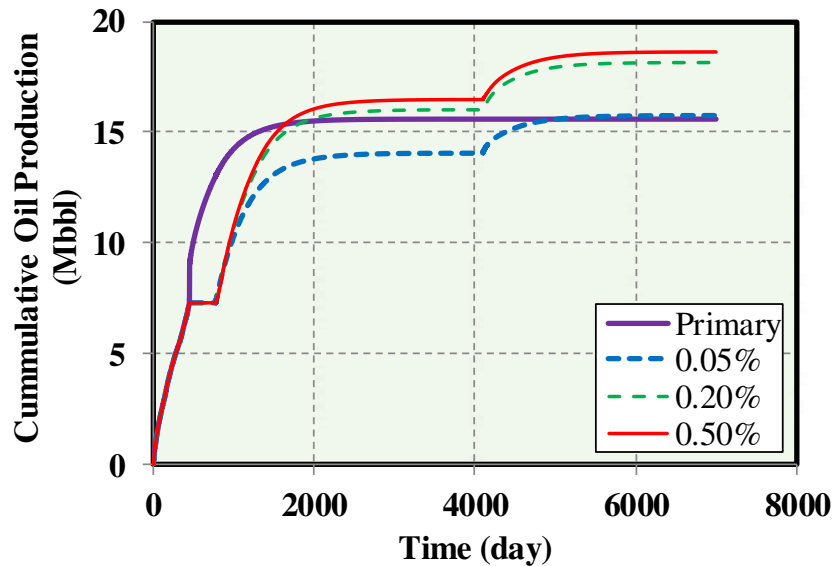


Fig. 55 Effect of surfactant concentration on surfactant Huff-n-Puff effectiveness.

To evaluate the relative impact of the parameters, the impacts of all uncertain parameters on the EOR effectiveness at 7000 days of production are shown in the Tornado plot (**Fig. 56**). It is clear that the number of surfactant Huff-n-Puff cycles and the surfactant concentration have an extreme effect on EOR. Moreover, it is followed by surfactant adsorption, soaking time, injection time and rate in order. This rank is based on the range of each parameter used in this study. The range for the incremental oil recovery factor at the time of 7000 days of production is about 1.1%-25.2%.

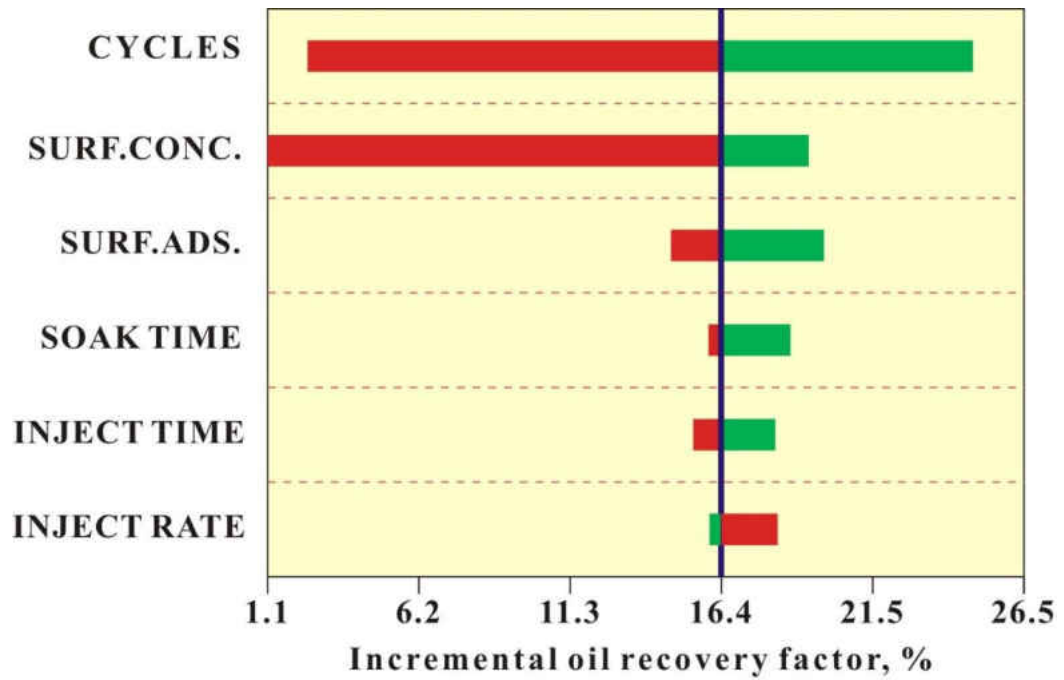


Fig. 56 Rank of impacts of six uncertain parameters on incremental oil recovery factor.

CHAPTER VI

CONCLUSIONS AND RECOMMENDATIONS

Enhanced oil recovery has been a hot topic over the past few decades. Due to the uncertainty of the technology and theory, Bakken is still stagnant at the stage of stimulation fracturing and has not injected anything to improve the oil recovery. The geology background is first investigated in this study. The geological experiments showed the porosity is about 4%, and pore diameter mainly distributed in the range from 4 μm to 40 μm . The pore throat diameter is between 0.8~2 μm . We found that the rock is mainly composed of dolomite and clay mineral, a part of calcite and a little silt detritus, it indicates lithology of the Middle Bakken formation is mainly dolomite and mudstone which can be characterized as a tight reservoir with low porosity and low permeability. The content of organic matter is low, it proves that the Middle Bakken layer is the main reservoir in Bakken Formation. Micropores are not developed well in organic matter, which in turn fully developed in interlamellar clay minerals. The microfractures hardly found in this area. The comparably good roundness of the particle and the particle size are smaller than 0.06mm but larger than 0.03mm. The structures of the particles is mainly grain structure and argillaceous structure.

Chapter IV presented a numerical compositional model in combination with the EDFM method to simulate CO₂ Huff-n-Puff in the tight oil reservoir with hydraulic fractures. This model is proper to be used in any unconventional tight oil reservoirs, not only Bakken. The fluid and gas properties, hydraulic fracture, model size and historical production data are

accurately considered. The fluid compositional model is validated through history matching with actual Middle Bakken tight oil. The effects of different CO₂ Huff-n-Puff parameters and CO₂ molecular diffusivity on the CO₂ Huff-n-Puff effectiveness were examined. The following conclusions can be drawn from this study:

1. The EDFM method has the same accuracy as the traditional LGR method for simulating the Middle Bakken tight oil reservoir, but the LGR method will take about 1.76 times of running time than the EDFM method.
2. The model and fluid properties used in this study are similar to the actual field case. There is an excellent agreement between historical production data and this simulation results. Both field model and section models can match the actual historical data.
3. With each case study, the history matching process was conducted first. With the good history match, the reservoir and fluid properties are incredibly close to the real case which means that the simulation study can be considered with the actual condition. So this study is meaningful for practical purposes to use as reference.
4. The case with 200 Mscf/day CO₂ injection rate, 50 injection days and 14 soaking days for each cycle, with three cycles at the 500th day, 2000th day and 4000th day, has the highest cumulative oil production that the recovery factor can reach 5.9%. The CO₂ molecular diffusion for this case is also the highest one which is 0.1 cm²/s.
5. Each case study with CO₂ Huff-n-Puff process has a positive effect on improved oil recovery factor, only the case with CO₂ molecular diffusion as 0.001 cm²/s has a negative effect. This phenomenon means that with the bad solubility, the gas

injection will not help to produce more oil. So the gas with lousy solubility will not be helpful for EOR process.

6. In this CO₂ Huff-n-Puff study, the contribution of each CO₂ Huff-n-Puff parameters to cumulative oil production after 7000 days can be ranked as sequence: CO₂ diffusivity (extremely), number of cycle (moderate extremely), CO₂ injection time (moderate), CO₂ injection rate (moderate slight), CO₂ soaking time (slight).
7. A good numerical tool (EDFM) is proposed in this study which can be used for the CO₂ Huff-n-Puff simulation in the tight oil reservoir with multiple hydraulic fractures more effective and faster.

Chapter V investigated the influence of surfactant on EOR. Depending on the amount of surfactant adsorbed to the rock surface, the wettability of the rock can be altered to varying degrees by changing the relative permeability and capillary pressure. The Langmuir-type isotherm curve was used to describe the surfactant adsorption. A numerical chemical flooding model (CMG-STARs) in combination with the EDFM method was proposed to simulate the surfactant flooding in tight oil reservoirs with hydraulic fractures. This model can not only be used in the Middle Bakken formation, but also in other unconventional tight oil reservoirs. The surfactant and fluid properties, wettability alteration, optimal model size, and historical production data were accurately considered. The fluid compositional model was validated through history matching with actual Middle Bakken tight oil. The effects of different surfactant Huff-n-Puff parameters and surfactant adsorption parameters on the surfactant Huff-n-Puff effectiveness were examined. The following conclusions can be made from this study:

1. The model and fluid properties used in this study are similar to the actual field case, and the grid size is also optimized by a grid sensitivity analysis. An excellent agreement achieved between the historical production data and the simulation results. Both field model and sector models can match the actual historical data.
2. The effect of surfactant EOR was simulated by considering the IFT reduction and the rock wettability alteration from oil-wet to water-wet according to the Langmuir-type isotherm curve of the adsorption of the surfactant concentration.
3. A surfactant effectiveness verification was conducted before the sensitivity studies, and an actual production process was conducted at the beginning of each sensitivity case study. With the effective surfactant flooding and good history match, the reservoir and fluid properties are incredibly close to the real case which means that the simulation study can be considered with the actual production process. Therefore, this surfactant flooding study is meaningful for practical workers to use for reference.
4. The case with three surfactant Huff-n-Puff cycles has the highest cumulative oil production that the percentage of recovery increase over the primary recovery can reach 25.2% and also for the case with the highest surfactant concentration which can reach 19.4% of the percentage of recovery increase over the primary recovery. Both of them have a high surfactant injection. Therefore, the amount of surfactant injected into the reservoir is the key to increasing production.
5. In this surfactant Huff-n-Puff study, the contribution of each surfactant Huff-n-Puff parameter to cumulative oil production after 7,000 days can be ranked into two groups: 1. The number of surfactant Huff-n-Puff cycles and surfactant

concentration. 2. Surfactant adsorption, injection time, soaking time, and injection rate. The parameters in the first group have more substantial effect on EOR, and the parameters on the other group only have a lighter effect.

6. EDFM method proposed in this study can simulate the wettability alteration and surfactant Huff-n-Puff process in the tight oil reservoirs with multiple hydraulic in a more straightforward and fast way.

REFERENCE

- Abdulkareem, M. A., Liu, J. S., Han, M., and Aramco, S., 2012. Numerical Simulation of Surfactant-Polymer Coreflooding Experiments for Carbonates. *Journal of Petroleum Science and Engineering* 111 (2013) 184-196.
- Adekunle, O., and Hoffman, B.T., 2014. Minimum Miscibility Pressure Studies in the Bakken. SPE 169077, SPE Improved Oil Recovery Symposium, Tulsa, Oklahoma, 12-16 April.
- Adibhatia, B. U., Sun, X. U., and Mohanty, K. U., 2005. Numerical studies of Oil Production from Initially Oil-Wet Fracture Blocks by Surfactant Brine Imbibition. SPE 97687, SPE International Improved Oil Recovery Conference, Kuala, Malaysia, 5-6 December.
- Adkins, S., Liyanage, P. J., Arachchilage, G. W., Mudiyansele, T., Weerasooriya, U., and Pope, G. A., 2010. A New Process for Manufacturing and Stabilizing High-Performance EOR Surfactant at Low Cost for High Temperature, High Salinity Oil Reservoirs. SPE 122923, SPE Improved Recovery Symposium, Tulsa, Oklahoma, 25-28 April.
- Alfarge, D., Wei, M., and Bai, B. 2017a. IOR Methods in Unconventional Reservoirs of North America: Comprehensive Review. SPE 185640, SPE Western Regional Meeting, Bakersfield, CA, 24-27 April.
- Alfarge, D., Wei, M., & Bai, B., 2017b. Factors Affecting CO₂-EOR in Shale-Oil Reservoirs: Numerical Simulation study and Pilot Test. *Journal of Energy&Fuel*. DOI: 10.1021/acs.energyfuels.7b01623.
- Alharthy, N., Teklu, T., Nguyen, T., Kazemi, H., and Graves, R., 2016. Nanopore Compositional Modeling in Unconventional Shale Reservoirs. *SPE Res. Eval & Eng.* 19 (3): 415-428. doi:<http://dx.doi.org/10.2118/166306-PA>.
- Anderson, G. A., 2006. Simulation of Chemical Flooding Enhanced Oil Recovery Processes Including the Effects of Reservoir Wettability. M.S thesis, The University of Texas at Austin, Texas.
- Atsushi, L., and Akhil D.G., 2018. Optimizing CO₂ and Field Gas Injection EOR in Unconventional Reservoirs Using the Fast Marching Method. SPE 190304, SPE Improved Oil Recovery Conference, Tulsa, Oklahoma, 14-18 April.
- Bonnie, J. H., and Fens, T. W., 1992. Porosity and Permeability from SEM Based Image Analysis of Core Material. SPE-23619, Caracas, Venezuela, 8-11 March.
- Bi, G. P., Chen, X. Y., Yang, Z., and Ma, A., 2018. The measuring method for actual total magnification of metallographic microscope-digital image method. *IOP Conference Series: Materials Science and Engineering* 397 (2018) 012148.
- Carlson, C. G., and Anderson, S. B., 1965. Sedimentary and Tectonic History of North Dakota Part of Williston Basin. *AAPG Bulletin*, v. 11, p. 1833-1846.
- Cavalcante Filho, J.S.A., Shakiba, M., Moinfar, A., and Sepehrnoori, K., 2015. Implementation of a Preprocessor for Embedded Discrete Fracture Modeling in an

- IMPEC Compositional Reservoir Simulator. SPE 173289, SPE Reservoir Simulation Symposium, Houston, Texas, 23-25 February.
- Chen, C., Balhoff, M., and Mohanty, K.K., 2014. Effect of Reservoir Heterogeneity on Primary Recovery and CO₂ Huff 'n' Puff Recovery in Shale-Oil Reservoirs. SPE Reservoir Evaluation and Engineering, 17 (3): 404-413.
- Cheraghian, G., Nezhad, S. S. L., Kamari, M., Hemmati, M., Masihi, M., and Bazgir, S., 2014. Adsorption Polymer on Reservoir Rock and Role of the Nanoparticles, Clay and SiO₂. International Nano Letters, 4: 114.
- Cipolla, C.L., and Wallace, J., 2014. Stimulated Reservoir Volume: a Misapplied Concept? Paper SPE 168596, SPE Hydraulic Fracturing Technology Conference, The Woodlands, Texas, 4-6 February.
- Clelland, W. D., and Fens, T. W., 1991. Automated Rock Characterization With SEM/Image-Analysis Techniques. SPE Formation Evaluation, December 1991.
- Cosima, T., and Stephen. A. S., 2013. Integrating Geology and Engineering: Implications for Production in the Bakken Play, Williston Basin. SPE 168870/URTeC 1596247, Unconventional Resource Technology Conference, Denver, Colorado, USA, 12-14 August.
- Cramar D. D., 1986. Reservoir characteristics and stimulation techniques in the Bakken Formation and adjacent beds, Billings Nose area, Williston Basin, in S. Goolsby and M. W. Longman, eds., Proceedings from SPE Rocky Mountain Region Technical Meeting. Society of Petroleum Engineers, paper no. 15166, p. 331-344.
- Cramar, D. D., 1991. Stimulation treatments in the Bakken Formation: Implications for horizontal completions, in W. B. Hansen, ed., Geology and horizontal drilling of the Bakken Formation: Montana Geological Society, p. 117-140.
- Crank, J., 1975. The Mathematics of Diffusion. Second edition, Clarendon Press, Oxford.
- Datta-Gupta, A., Pope, G. A., Sepehrnoori, K., and Thrasher, R. L., 1986. A Symmetric, Positive Definite Formulation of a Three-Dimensional Micellar/Polymer Simulator. SPE Reservoir Engineering 1, No. 6, Pages: 622-632.
- David R.M., West J.H., Monte R., Besler M.B., and Kenneth D.M., 2013. Optimized Production in the Bakken Shale: South Antelope Case Study. SPE 167168, SPE Unconventional Resources Conference-Canada, Calgary, Alberta, Canada, November 5-7.
- Dawson, M., Nguyen, D., Champion, N., and Li, H. N., 2015. Designing an Optimized Surfactant Flooding in the Bakken. SPE 175937, SPE/CSUR Unconventional Resources Conferences held in Calgary, Alberta, Canada, 20-22 October.
- Delshad, M., Pope, G. A., and Sepehrnoori, K., 1996. A Compositional Simulator for Modeling Surfactant Enhanced Aquifer Remediation. Journal of Contaminant Hydrology, 23, 303-327.
- Division of Mineral Resources, 2018 retrieved from: <https://www.dmr.nd.gov/oilgas/stats/historicalbakkenoilstats.pdf>.
- Dow, W. G., 1974. Application of oil-correlation and source-rock data to exploration in Williston Basin. AAPG Bulletin, v. 58, p. 1253-1262.
- DuBose, K., 2012. Bakken Shale Play, <http://bakkenshale.com>, Accessed July 20, 2018.
- Gaswirth, S.B., and Marra, K., 2013. Assessment of Undiscovered Oil Resources in the Bakken and Three Forks Formations, Williston Basin Province, Montana, North

- Dakota, and South Dakota. USGS National Assessment of Oil and Gas Fact Sheet: 2013-2013, 4 p.
- Gorgan, A.T., and Pinczewski, W.V., 1986. The Role of Molecular Diffusion Processes in Tertiary Carbon Dioxide Flooding. *JPT*: 591-602.
- Government of Saskatchewan., 2015. Energy Briefing Note: The Ultimate Potential for Unconventional Petroleum from the Bakken Formation of Saskatchewan. <http://www.neb-one.gc.ca/nrg/sttstc/crdlndptrlmprdct/rprt/2015bkkn/index-eng.html>.
- Haines, H.K., and Monger, T.G., 1990. A Laboratory Study of Natural Gas Huff 'N' Puff. SPE-21576, CIM/SPE International Technical Meeting. Calgary, Alberta, 10-13 June.
- Hajibeygi, H., Karvounis, D., and Jenny, P., 2011. A Hierarchical Fracture Model for the Iterative Multiscale Finite Volume Method. *K. Comput. Phys.* 230 (24): 8729-8743.
- Jacobs, T., 2015. Unconventional Resources Will Require Unconventional EOR. *J. Pet Tech*, 67 (09): 68-70.
- Jiang, J., Shao, Y., and Younis, R. M., 2014. Development of a Multi-Continuum Multi-Component Model for Enhanced Gas Recovery and CO₂ Storage in Fractured Shale Gas Reservoirs. SPE 169114, SPE Improved Oil Recovery Symposium, Tulsa, 12-16 April.
- Jung, H. Y., Onishi, T., and Datta-Gupta, A., 2018. Numerical Simulation of EOR from Wettability Alteration in Tight Oil Reservoir with Multiple Hydraulic Fractures. SPE 191409, SPE Annual Technical Conference and Exhibition, Dallas, Texas, 24-26 September.
- Kurtoglu, B., and Kazemi, H., 2012. Evaluation of Bakken Performance Using Coreflooding, Well Testing, and Reservoir Simulation. SPE 155655, SPE Annual Technical Conference and Exhibition, San Antonio, TX, 8-10 October.
- Kurtoglu, B., Sorensen, J.A., Barunberger, J., Smith, S., and Kazemi, H., 2013. Geologic Characterization of a Bakken Reservoir for Potential CO₂ EOR. Paper URTeC 1619698, presented at the Unconventional Resources Technology Conference, Denver, Colorado, 12-14 August.
- Land, C. S., 1971. Comparison of Calculated with Experimental Imbibition Relative Permeability. *SPE J.*, 11(4), 419-425.
- Lee, S. H., Lough, M. F., and Jensen, C. L., 2001. Hierarchical Modeling of Flow in Naturally Fractured Formations With Multiple Length Scales. *Water Resour. Res.* 37 (3): 443-455.
- LeFever, J. A., 2007. Evolution of oil production in the Bakken formation: RMS-AAPG meeting and NDIC Geologic Investigation 49, NDIC website PowerPoint presentation, <https://www.dmr.nd.gov/ndgs/bakken/papers/petroleum%20Council%202004.ppt> Accessed December 15, 2008.
- LeFever, J. A., Martiniuk, C. D., Dancsok, E. F. R., and Mahnic, P. A., 1991. Petroleum potential of the middle member, Bakken Formation, Williston Basin, in J. E. Christopher and F. Haidl, eds., *Proceedings of the Sixth International Williston Basin Symposium: Saskatchewan Geological Society, Special Publication 11*, p. 74-94.
- Le, N.S., Hatakeyma, A., Farag, S., Konishi, Y., Vo, V.H., Takagi, S., and Phan, N.T., 2013. Fluid Saturation Monitoring by Cased Hole Logging for CO₂ Huff-n-Puff Test in a Vietnam Offshore Field. SPE 165236, SPE Enhanced Oil Recovery Conference, Kuala Lumpur, Malaysia, 2-4 July.

- Liu, J. J., Lin, L. J., and Ji, Y. J., 2011. Using Rock SEM Image to Create Pore-scale Finite Element Calculation Mesh. International Conference on Physics Science and Technology (ICPST 2011).
- Lotfollahi, M., Beygi, M. R., Abouie, A., Sepehrnoori, K., Wheeler, M. F., and DiCarlo, D. A., 2017. Optimization of Surfactant Flooding in Tight Oil Reservoirs. URTeC 2696038, Unconventional Resources Technology Conference, Austin, Texas, USA, 24-26, July.
- Lu, J., 2014. Development of Novel Surfactants and Surfactant Methods for Chemical Enhanced Oil Recovery. PhD dissertation, The University of Texas at Austin, Texas, August.
- Masalmeh, S.K., 2002. The Effect of Wettability on Saturation Functions and Impact on Carbonate Reservoir in the Middle East. SPE 78515, Society of Petroleum Engineers.
- Matthai, S., Menzentsev, A., and Belayneh, M., 2005. Control-Volume Finite-Element Two-Phase Flow Experiments With Fractured Rock Represented by Unstructured 3D Hybrid Meshes. SPE 93341, SPE Reservoir Simulation Symposium, The Woodlands, Texas, 31 January-2 February.
- Meissner, F. E., 1978. Petroleum geology of the Bakken formation, Williston Basin, North Dakota and Montana, in D. Estele, and R. Miller, eds., The economic geology of the Williston Basin, 1978 Williston Basin Symposium, Montana Geological Society, p. 207-230.
- Meissner, F. F., and Banks, R. B., 2000. Computer simulation of hydrocarbon generation, migration, and accumulation under hydrodynamic conditions – examples from the Williston and San Juan Basins, USA. AAPG Search and Discovery Article #40179, <http://www.searchanddiscovery.net/documents/2005/banks/index.htm?q=%3Ameissner> Accessed December 15, 2008.
- Mohammad, L., Mohammad, R. B., Ali, Abouie, A., Sepehrnoori, K., Wheeler, M. F., and DiCarlo, D. A., 2017. Optimization of Surfactant Flooding in Tight Oil Reservoirs. URTeC:2696038, Austin, Texas, USA, 24-26, July 2017.
- Moinfar, A., Varavei, A., Depehrnoori, K., et al., 2014. Development of Coupled Dual Continuum and Discrete Fracture Model for the Simulation of Unconventional Reservoirs. SPE 163647, SPE Reservoir Simulation Symposium, Woodlands, Texas, 18-20 February.
- Moinfar, A., Varavei, A., Sepehrnoori, K., and Johns R. T., 2014. Development of an Efficient Embedded Discrete Fracture Model for 3D Compositional Reservoir Simulation in Fractured Reservoirs. SPE Journal, 19(2):289-303.
- Mojdeh, D., Pope, D. A., and Sepehrnoori, K., 1996. A Compositional Simulator for Modeling Surfactant Enhanced Aquifer Remediation. Journal of Contaminant Hydrology, 23, 303-327.
- Monger, T., and Coma, J., 1988. A laboratory and field evaluation of the CO₂ Huff'n'Puff process for lightoil recovery. SPE 15501, SPE reservoir engineering 3 (04): 1168-1176.
- Murray, G. H., 1968. Quantitative fracture study – Sanish Pool, McKenzie County, North Dakota. AAPG Bulletin, v. 52, no. 1, p. 57-65.
- Ngo, I., Srisuriyachai, F., Sugai, Y., and Sasaki, K., 2017. Study of Heterogeneous Reservoir Effects on Surfactant Flooding in Consideration of Surfactant Adsorption Reversibility. Formation Evaluation Symposium, Japan.

- North Dakota Oil and Gas Commission (NDIC)., 2012. ND Monthly Bakken Oil Production Statistics.
- Panfili, P., and Cominelli, A., 2014. Simulation of Miscible Gas Injection in a Fractured Carbonate Reservoir Using an Embedded Discrete Fracture Model. SPE 171830, Abu Dhabi International Petroleum Exhibition and Conference, Abu Dhabi, 10-13 November.
- PGE (Editor), 2007. Technical Documentation for Utchem-9.0, a Three-Dimensional Chemical Flood Simulator, II. Reservoir Engineering Research Program, Center for Petroleum and Geosystems Engineering, The University of Texas at Austin, 256 pp.
- Pitman, J. K., Price, L. C., and LeFever, J. A., 2001. Diagenesis and fracture development in the Bakken Formation, Williston Basin: Implications for reservoir quality in the middle member. US Geological Survey Professional Paper 1653, 19 p.
- Pollarstro, R. M., Cook, T. A., Roberts, L. N. R., Schenk, C. J., Lewan, M. D., Anna, L. O., Gaswirth, S. B., Lillis, P. G., Klett, T. R., and Charpentier, R. R., 2008. Assessment of undiscovered oil sources in the Devonian-Mississippian Bakken Formation, Williston Basin Province, Montana and North Dakota: U. S. Geological Survey Fact Sheet, 2008-3021, 2p.
- Ponomarev, A. A., Mamadaliev, R. A., and Semenova, T. V., 2016. Tomography in Geology: 3D Modeling and Analysis of Structural Feature of Rock Using Computed Micro-Tomography. IOP Conference Series: Materials Science and Engineering 154(2016) 012030.
- Price, L. C., and LeFever, J. A., 1994. Dysfunctionism in the Williston basin: the mid-Madison/Bakken petroleum system. Bulletin of Canadian Petroleum Geology, v. 42, no. 2, p. 187-218.
- Price, L. C., and Stolper, K., 1999. Evidence and causes of super-lithostatic fracturing, in L. C. Price, Origins and characteristics of the basin-center continuous-reservoir unconventional oil-resource base of the Bakken Source System, Williston Basin, p. 108-136. Accessed May 6, 2010 <http://www.undeerc.org/Price/>.
- Sanchez, R. D., 2014. Reservoir simulation and optimization of CO₂ huff-and-puff operations in the Bakken shale [MS thesis]. Austin, TX: The University of Texas at Austin.
- Sandve, T. H., Berre, I., and Nordbottem, J. M., 2012. An Efficient Multi-Point Flux Approximation Method for Discrete Fracture-Matrix Simulations. Journal of Computational Physics 231(9): 3784-3800.
- Schmoke, J. W., and Hester, T. C., 1983. Organic carbon in Bakken Formation, United States portion of Williston Basin: AAPG Bulletin, v. 67, p. 2165-2174.
- Shakiba, M., and Sepehrnoori, K., 2015. Using Embedded Discrete Fracture Model (EDFM) and Microseismic Monitoring Data to Characterize the Complex Hydraulic Fracture Networks. SPE 175142, SPE Annual Technical Conference and Exhibition, Houston, Texas, 28-30 September.
- Sharma, G., and Mohanty, K. K., 2013. Wettability Alteration in High-Temperature and High-Salinity Carbonate Reservoirs. SPE 147306, SPE Annual Technical Conference and Exhibition, Denver, Colorado, 30 October-2 November.
- Shoaib, S., and Hoffman, B.T., 2009. CO₂ Flooding the Elm Coulee Field. SPE 123176, SPE Rocky Mountain Petroleum Technology Conference, Denver, Colorado, 14-16 April.

- Singh, R., and Mohanty, K. K., 2016. Foams With Wettability-Altering Capabilities for Oil-Wet Carbonates: A Synergistic Approach. SPE Journal.
- Smith, M. G., and Bustin, M., 1996. Lithofacies and paleoenvironments of the upper Devonian and lower Mississippian Bakken Formation, Williston Basin. Bulletin of Canadian Petroleum Geology, v. 44, no. 3, p. 495-507.
- Song, C., and Yang, D., 2013. Performance Evaluation of CO₂ Huff-n-Puff Processes in Tight Oil Formations. Paper SPE 167217, SPE Unconventional resources Conference, Alverta, Canada, 5-7 November.
- Song, S. X., Xing, A., and Zhao, J., 2002. Influence of Microscopy Amplifying Multiple on the Measurement of Fracture Toughness [J]. Materials Science and Engineering, 78 (2): 251-253.
- Sorensen, J. A., Jason, R. B., Liu, G.X., Steven A. S., Robert, C. K., Edward, N. S., and John, A. H., 2014. CO₂ storage and utilization in tight hydrocarbon-bearing formations: a case study of the Bakken Formation in the Williston Basin. Energy Procedia, 63 (2014): 7852-7860.
- Stephen, A. S., Julie, A. L., and Ronald, J. H., 2011. The Bakken-Three Forks Petroleum System in the Williston Basin. Chapter 15.
- Sun, R., Yu, W., Xu, F., Pu, H., and Miao, J., 2019. Compositional simulation of CO₂ Huff-n-Puff process in Middle Bakken tight oil reservoir with hydraulic fracture. Journal of Fuel, 236 (2019):1446-1457.
- Tabary, R., Bazin, B., Douarche, F., Moreau, P., and Oukhemanou-Destremaut, F., 2013. Surfactant Flooding in Challenging Conditions: Towards Hard Brines and High Temperature. SPE 164359, SPE Middle East Oil and Gas Show and Conference, Manama, Bahrain, 10-13 March.
- Turgay, E., Jamal H., and Gregory, R., 2001. Basic Applied Reservoir Simulation. Henry L. Doherty Memorial Fund of AIME Society of Petroleum Engineers. Richardson, Texas.
- Vakhrusheva, I. A., Gilmanov, Y. I., and Patrakov, D. P., 2015. Digital core-new area of petrophysical core analysis. Current state in Russia and in the world. Proceedings of the 5th research and applied science conference Supercomputer technologies in the oil and gas industry. Mathematical methods, software and hardware. 112-16.
- Wang, J., Han, M., Fuseni, A. B., and Cao D., 2015. Surfactant Adsorption in Surfactant-Polymer Flooding for Carbonate Reservoirs. SPE 172700, SPE Middle East Oil & Gas Show and Conference, Manama, Bahrain, 8-11 March.
- Wan, T., and Sheng, J., 2015. Compositional Modeling of the Diffusion Effect on EOR Process in Fractured Shale-Oil Reservoirs by Gasflooding. J. Cdn. Pet. Tech. 54 (2): 107-115. doi:<https://doi.org/10.2118/2014-1891403-PA>.
- Wang, X., Luo, P., Er, V., and Huang, S., 2010. Assessment of CO₂ Flooding Potential for Bakken Formation, Saskatchewan. SPE 137728, Canadian Unconventional Resources and International Petroleum Conference, Calgary, Canada, 19-21 October.
- Williams, J. A., 1974. Characterization of oil types in Williston basin. AAPG Bulletin, v. 58, p. 1243-1252.
- Wu, K., and Olson, J.E., 2016. Numerical Investigation of Complex Fracture Networks in Naturally Fractured Reservoirs. SPE Production & Operations, 31 (4): 300-309.

- Xu, Y., 2015. Implementation and Application of the Embedded Discrete Fracture Model (EDFM) for Reservoir Simulation in Fractured Reservoirs. Master Thesis, The University of Texas at Austin, Austin, Texas.
- Xu, Y., Cavalcante Filho, J.S.A., Yu, W., and Sepehrnoori, K., 2017a. Discrete-Fracture Modeling of Complex Hydraulic-Fracture Geometries in Reservoir Simulators. SPE Reservoir Evaluation & Engineering, 20 (2): 403-422.
- Xu, Y., Yu, W., and Sepehrnoori, K., 2017b. Modeling Dynamic Behaviors of Complex Fractures in Conventional Reservoir Simulators. Paper URTEC 2670513, presented at the SPE/AAPG/SEG Unconventional Resources Technology Conference, Austin, Texas, 24-26 July.
- Yang, H., Li, J., Jiang, H., Hu, J., and Zeng, J., 2018. Alkaline-Surfactant-Polymer Flooding: Where is the Enhanced Oil Exactly. SPE 190340, SPE EOR Conference at Oil and Gas West Asia, Muscat, Oman, 26-28 March.
- Yu, W., Al-Shalabi, E. W., and Sepehrnoori, K., 2014. A Sensitivity Study of Potential CO₂ Injection for Enhanced Gas Recovery in Barnett Shale Reservoirs. SPE 169012, SPE Unconventional Resources Conference, Woodlands, Texas, 1-3 April.
- Yu, W., Lashgari, H and Sepehrnoori, K., 2014a. Simulation Study of CO₂ Huff-n-Puff Process in Bakken Tight Oil Reservoirs. SPE 169575, SPE Western North American and Rocky Mountain Joint Regional Meeting held in Denver, Colorado, USA, 16-17 April.
- Yu, W., Huang, Shan., Wu, Kan., Sepehrnoori, K and Zhou, W. 2014b. Development of a Semi-Analytical Model for Simulation of Gas Production in Shale Gas Reservoirs. URTEC-1922945-MS, presented at the Unconventional Resource Technology Conference held in Denver, Colorado, USA, 25-27 August 2014.
- Yu, W., Xu, Y., Weijermars, R., Wu, K., and Sepehrnoori, K., 2017. A Numerical Model for Simulating Pressure Response of Well Interference and Well Performance in Tight Oil Reservoirs With Complex-Fracture Geometries Using the Fast Embedded-Discrete-Fracture-Model Method. SPE Reservoir Evaluation & Engineering, in press.
- Yu, W., Lashgari, H., Wu, K., and Sepehrnoori, K., 2015. CO₂ injection for enhanced oil recovery in Bakken tight oil reservoirs. Fuel 2015; 159:354-63.
- Yu, W., and Sepehrnoori, K., 2018. Shale Gas and Tight Oil Reservoir Simulation, 1st Ed.; Publisher: Elsevier, Cambridge, USA. ISBN: 978-0-12-813868-7.
- Yu, W., Zhang, Y., Sepehrnoori, K and Zhang, T. 2018. Compositional Simulation of CO₂ Huff-n-Puff in Eagle Ford Tight Oil Reservoirs with CO₂ Molecular Diffusion, Nanopore Confinement and Complex Natural Fractures. SPE 190325, SPE Improved Oil Recovery Conference held in Tulsa, Oklahoma, USA, 14-18 April.
- Yuan, S. Y., Yang, P. H., Dai, Z. Q., and Shen, K. Y., 1995. Numerical Simulation of Alkali/Surfactant/Polymer Flooding. SPE 29904.
- Yuan, Y., and Lee, T. R., 2013. Contact Angle and Wetting Properties. Surface Science Techniques, Vol. 51 of the series Springer Series in Surface Sciences, Pages: 3-34.
- Yue, K., J. E. Olson, and R. A. Schultz (2018), Layered modulus effect on fracture modeling and height containment, paper 2898691 to be presented at the Unconventional Resources Technology Conference, Houston, Texas, July 23–25, 2018.
- Zhang, Y., Yuan, D., Yu, W., and Sepehrnoori, K., 2017. A comprehensive model for investigation of CO₂-EOR with nanopore confinement in the Bakken tight oil reservoir.

- SPE 187211, SPE Annual Technical Conference and Exhibition, San Antonio, Texas, 9-11 October.
- Zuloaga, P., Yu, W., Miao, J., and Sepehrnoori, K., 2017. Performance evaluation of CO₂ huff-n-puff and Continuous CO₂ injection in tight oil reservoir. *Energy* 134, 181-192.
- Zuloaga, P., Yu, W., Xu, Y., Sepehrnoori, K., and Li, B., 2016. Simulation study of CO₂-EOR in tight oil reservoirs with complex fracture geometries. *Sci. Rep.* 6, 33445.